

1

AD-A164 214



TWO-DIMENSIONAL CONFINED JET THRUST
 VECTOR CONTROL WITH FLOW VISUALIZATION
 AND VARIABLE FLOW GEOMETRY

THESIS

James W. Cates
 Captain, USAF

AFIT/GAE/AA/85D-2

DTIC FILE COPY

DISTRIBUTION STATEMENT A
 Approved for public release
 Distribution Unlimited

DTIC
SELECTED
FEB 13 1986

S D

B

DEPARTMENT OF THE AIR FORCE
 AIR UNIVERSITY
AIR FORCE INSTITUTE OF TECHNOLOGY

Wright-Patterson Air Force Base, Ohio

86 2 12 072

AFIT/GAE/AA/85D-2

TWO-DIMENSIONAL CONFINED JET THRUST
VECTOR CONTROL WITH FLOW VISUALIZATION
AND VARIABLE FLOW GEOMETRY

THESIS

James W. Cates
Captain, USAF

AFIT/GAE/AA/85D-2

Approved for public release; distribution unlimited

S DTIC
ELECTE **D**
FEB 13 1986
B

AFIT/GAE/ AA /85D-2

TWO-DIMENSIONAL CONFINED JET THRUST
VECTOR CONTROL WITH FLOW VISUALIZATION
AND VARIABLE FLOW GEOMETRY

THESIS

Presented to the Faculty of the School of Engineering
of the Air Force Institute of Technology

Air University

In Partial Fulfillment of the
Requirements for the Degree of
Master of Science in Aeronautical Engineering

James W. Cates, B.M.E.

Captain, USAF

December 1985

Approved for public release; distribution unlimited

Preface

In this thesis, I have attempted to define basic design criterion for a two-dimensional confined jet thrust vector control nozzle. Since theoretical analysis to date has been limited to three-dimensional confined jet thrust vector control, an empirical approach was followed in order to establish two-dimensional design parameters. In addition, schlieren photography was used to provide a visual record of flow behavior inside the nozzle.

I wish to thank Dr. M. E. Franke for his advice and patience throughout the course of this study. The technical efforts of the laboratory technicians and the AFIT shop cannot go without mention, especially those of Messrs. Nick Yardich, Leroy Cannon, Jay Anderson, Carl Shortt, and John Brohas. Special thanks to Phyllis Reynolds for her efforts in typing this thesis. And finally, thanks to Capt. Bobby Brown whose comic inspiration made preparing this thesis an enjoyable experience.

— James W. Cates

Accession For	
DTIC GRA&I	<input checked="" type="checkbox"/>
DTIC TAB	<input type="checkbox"/>
Unannounced	<input type="checkbox"/>
Justification	
Distribution	
Availability	
Dist	Special
A-1	



Table of Contents

	Page
Preface	ii
List of Figures	v
List of Tables	vii
List of Symbols	viii
Abstract	x
I. Introduction and Design Approach	1
Background	1
Boundary Layer Thrust Vector Control	1
Combined Jet Thrust Vector Control	2
Development of CJTVC	2
Purpose	4
Approach	4
II. Nozzle Design	5
Design Philosophy	5
SI Port Location	5
III. Experimental Apparatus	9
Test Assembly	9
Plexiglass Nozzle Shapes	11
Test Stand	11
SI System and Pressure Measurement	11
Mass Flow Measurement	12
Data Acquisition	12
Control	17
Flow Visualization System	17
IV. Experimental Procedure	20
V. Results and Discussion	22
Separation Characteristics	22
Determination of Separation Points	22
Comparison with Previous Studies	22

	Page
Nozzle Instabilities and Operating Modes	27
Exit-to-Throat Area Ratio Effects on Flow Stability	29
SI Effects on Vectored Flows	33
Geometric Effects on Vector Forces and Angles	33
Effects of Varying Axial Length	33
Effect of Varying Primary Pressure	37
Effects of Varying Exit-to-Throat Area Ratio	41
Two-Dimensional CJTVC Performance	41
Comparison to Ideal Performance	41
Performance with SI	41
VI. Conclusions	47
VIII. Recommendations	48
Appendix A: Mass Flow Calculations	49
Appendix B: Ideal Thrust Calculation	52
Bibliography	53
Vita.	54

List of Figures

Figure	Page
1. Boundary Layer Thrust Vector Control	3
2. Confined Jet Thrust Vector Control	3
3. Nozzle Schematic	6
4. Nozzle Components	10
5. Test Stand Schematic	13
6. Nozzle Mounted on Tank/Settling Chamber	14
7. Nozzle Mounted on Load Cell	15
8. Load Cell	16
9. Schematic of Schlieren System	18
10. Nozzle Wall Separation	23
11. Separation Distance Comparison	25
12. Schematic of Pressure Tap Locations	26
13. Pressure Profile for $A_e/A_t = 5$ with SI	30
14. Pressure Profile for $A_e/A_t = 3$	31
15. Schlieren Photographs for $A_e/A_t = 3$ Nozzle	32
16. SI Effect on $A_e/A_t = 5$ Nozzle	34
17. SI Effect on Side Force for Attached Flows	35
18. Primary Pressure Effects on Axial Force	38
19. Primary Pressure Effects on Side Force	39
20. Primary Pressure Effects on Vector Angle	40
21. SI Effect on Axial Force $A_e/A_t = 4$ and $L = 0$	42
22. SI Effect on Side Force $A_e/A_t = 4$ and $L = 0$	43

Figure	Page
23. SI Effect on $\alpha - A_e/A_t = 4$ and $L = 0$	44
24. Schlieren Photographs of $A_e/A_t = 4$, $L = 0$ Vector Operation	45

List of Tables

Table		Page
I.	Wall Pressure Data	24
II.	Nozzle Operating Modes	28
III.	Axial Length Effects on Operating Parameters .	36
IV.	Performance Comparisons	46

List of Symbols

<u>Symbols</u>	<u>Quantity</u>	<u>Units</u>
A	Cross-sectional area	in ²
C _T	Thrust coefficient	dimensionless
d	Orifice diameter	in
d'	Distance along nozzle wall from throat	in
D	Inside pipe diameter	in
I	Venturi flow constant	dimensionless
k	Ratio of specific heats	dimensionless
K	Orifice flow coefficient	dimensionless
L	Axial length variation	in
\dot{m}	Mass flow rate	lbm/s
M	Mach number	dimensionless
n	Velocity profile power law index	dimensionless
P	Pressure	psig
t	Throat depth	in
T	Temperature	deg R
Y ₁	Expansion factor	dimensionless
α	Vector angle	deg
η	Thrust ratio	dimensionless
γ	Nozzle inlet angle	deg
ρ_1	Fluid density	lbm/ft ³

<u>Symbols</u>	<u>Quantity</u>	<u>Units</u>
σ	Reconvergence angle	deg
θ	Nozzle wall divergence	deg

Subscripts

a	Ambient
avg	Average
e	Exit
f	Fluid
I	Ideal
m	Maximum
o	Supply
p	Primary
R	Reaction
si	Secondary injection
t	Throat

Abstract

An experimental investigation of a two-dimensional confined jet thrust vector control nozzle was performed. The performance parameters considered were axial force, side force, and vector angle. Flow visualization was used to provide a visual record of flow behavior. Variables included primary pressure, exit-to-throat area ratio, and exit-to-throat axial length.

With each test configuration, it was possible to define specific operating modes where the flow was oscillatory, vectored/switchable, and vectored/unswitchable. Only one test configuration yielded a stable axial flow on which secondary injection could be used to study vectoring. Switchable flows existed only at low pressures below the range of test pressures making it impossible to study switching characteristics. Because the flows were attached over the entire range of test pressures, geometric effects were based on the study of these attached flows.

Results indicate that the theoretical equations for predicting wall separation points in unconfined nozzles do not accurately predict the separation points in confined jet nozzles. Small variations in axial length as examined in this study had a minimal impact on nozzle performance. Primary pressure and exit-to-throat area ratio have the most significant impact on two-dimensional nozzle performance.

TWO-DIMENSIONAL CONFINED JET THRUST VECTOR
CONTROL WITH FLOW VISUALIZATION
AND VARIABLE FLOW GEOMETRY

I. Introduction and Design Approach

Background

Thrust Vector Control (TVC) represents a possible alternative to hydraulically controlled, gimballed nozzles in missile/space applications. This would result in weight and cost savings due to reduced system complexity. The basic theory of TVC is that the flow in an overexpanded nozzle can be forced off-axis to create a side force.

Boundary Layer Thrust
Vector Control

One proven method of TVC is Boundary Layer Thrust Vector Control (BLTVC), Figure 1. With BLTVC, secondary injectant (SI) in the form of ambient air, is allowed to enter into the separation region in an overexpanded flow, causing the flow to vector off-axis (Ref 1). A system of this type is dependent on ambient pressure greater than the pressures in the separation region for proper operation. Thus, BLTVC is limited to low-altitude operation. For high-altitude operation, a system is needed that can operate independently of altitude.

Combined Jet Thrust Vector Control

Confined Jet Thrust Vector Control (CJTVC) provides for operation at high altitudes. The design of a CJTVC nozzle is similar to that of a BLTVC nozzle except for the addition of a reconvergent section downstream of the over-expanded nozzle. This design contains the separation region within the body of the nozzle as shown in Figure 2. By having the flow exit the nozzle at supersonic speeds, the separation region operates independently of ambient conditions. Secondary injection is provided by a separate, independent supply which is used to switch the flow.

Development of CJTVC

CJTVC was studied extensively by Fitzgerald and Kampe at Chandler Evans Control Systems where the basic operation was proven in two-dimensional form (Ref 2). This initial work involved a BLTVC nozzle and provided for follow-on, three-dimensional studies. This effort continued through the 1970s. By measuring the geometric effects on side force and axial thrust, Fitzgerald and Kampe were able to develop three-dimensional design data which was published in 1980 (Ref 3). Fitzgerald and Kampe examined various geometric parameters; however, extensive study was performed to determine optimum SI port location, throat-to-exit orifice axial spacing and orifice-to-throat area ratio. Porzio (Ref 4) provided further study of

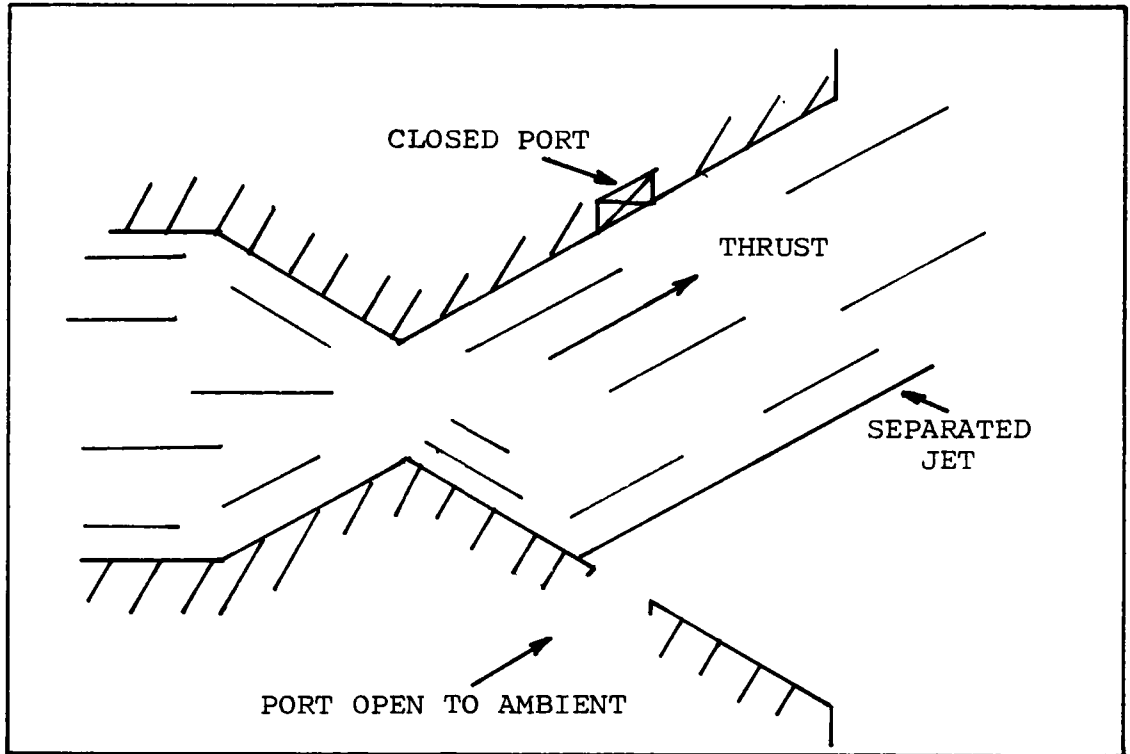


Figure 1. Boundary Layer Thrust Vector Control

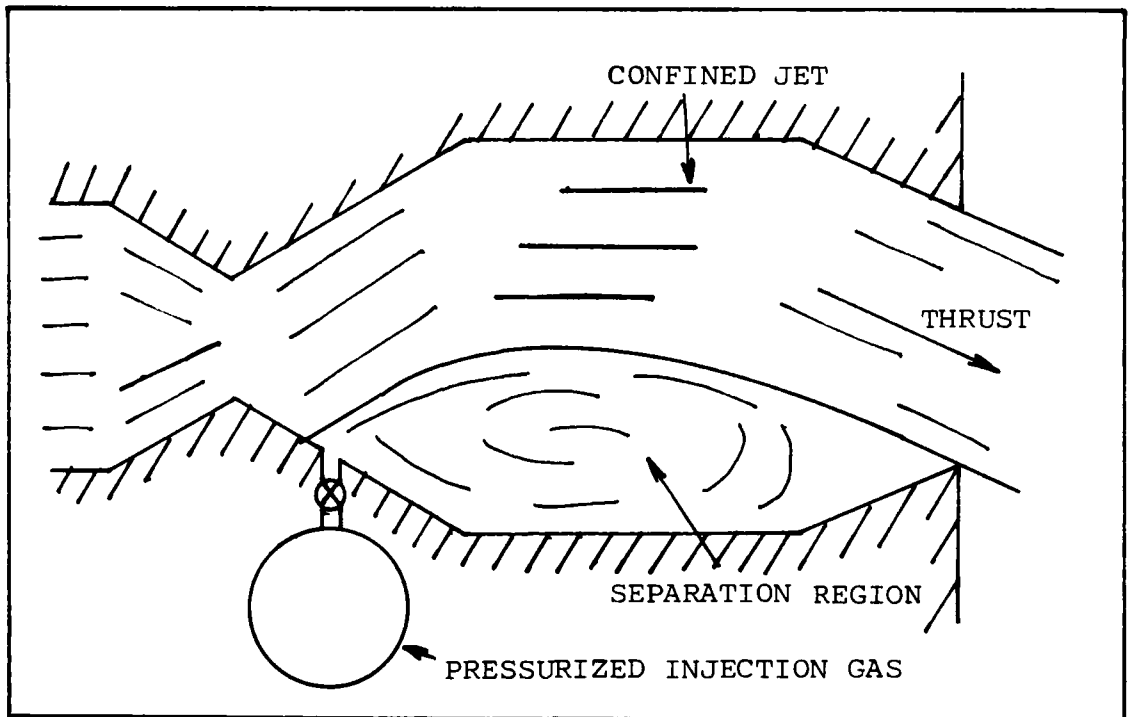


Figure 2. Confined Jet Thrust Vector Control

axisymmetric CJTVC nozzles examining the effects of varying primary and secondary pressure and control port cross-sectional area. Brown (Ref 5) continued with Porzio's work in parallel with this study. He studied the effects of varying exit-to-throat area ratio and exit-to-throat axial length.

Purpose

The purpose of this study was to perform a two-dimensional analysis of a CJTVC nozzle in parallel with the three-dimensional study performed by Brown. By working in two dimensions, flow visualization was convenient for studying the effects of confinement on flow separation, and the behavior of the vectored flow. In addition, the effects of varying axial length, exit-to-throat area ratio, and primary pressure were studied. These variables paralleled those being considered by Brown.

Approach

The approach taken was to design a two-dimensional nozzle with the capability to vary exit-to-throat area ratio and axial length. Each nozzle configuration was tested at primary pressures of 100, 150, and 200 psig. The test apparatus incorporated the capability to measure axial and side forces, vector angles and primary/secondary mass flow rate.

II. Nozzle Design

Design Philosophy

The three-dimensional guidelines established by Fitzgerald and Kampe were not appropriate for a two-dimensional nozzle. Since this effort was being performed in conjunction with Brown, it was decided to construct a two-dimensional nozzle with divergence angle and throat area that closely approximated Brown's (Ref 5). Maximum expansion ratio was determined by comparing various expansion heights to the maximum diameter used by Brown. This approach yielded a nozzle with a 20 deg divergence half-angle, a maximum expansion ratio of 12:1, and a throat height of 0.25 in. Nozzle depth was fixed at 0.75 in. Figure 3 shows a schematic of the basic nozzle. Nozzles with exit-to-throat area ratios of 3, 4, and 5 were tested. In addition, for each area ratio, axial lengths of the constant area section of 0.0, 0.5, and 1.0 in were examined. Reconvergence angle was held fixed at 45 deg for each configuration.

SI Port Location

SI port location for optimum performance was determined by Fitzgerald and Kampe (Ref 3) for three-dimensional nozzles. Their research indicated that optimum SI port

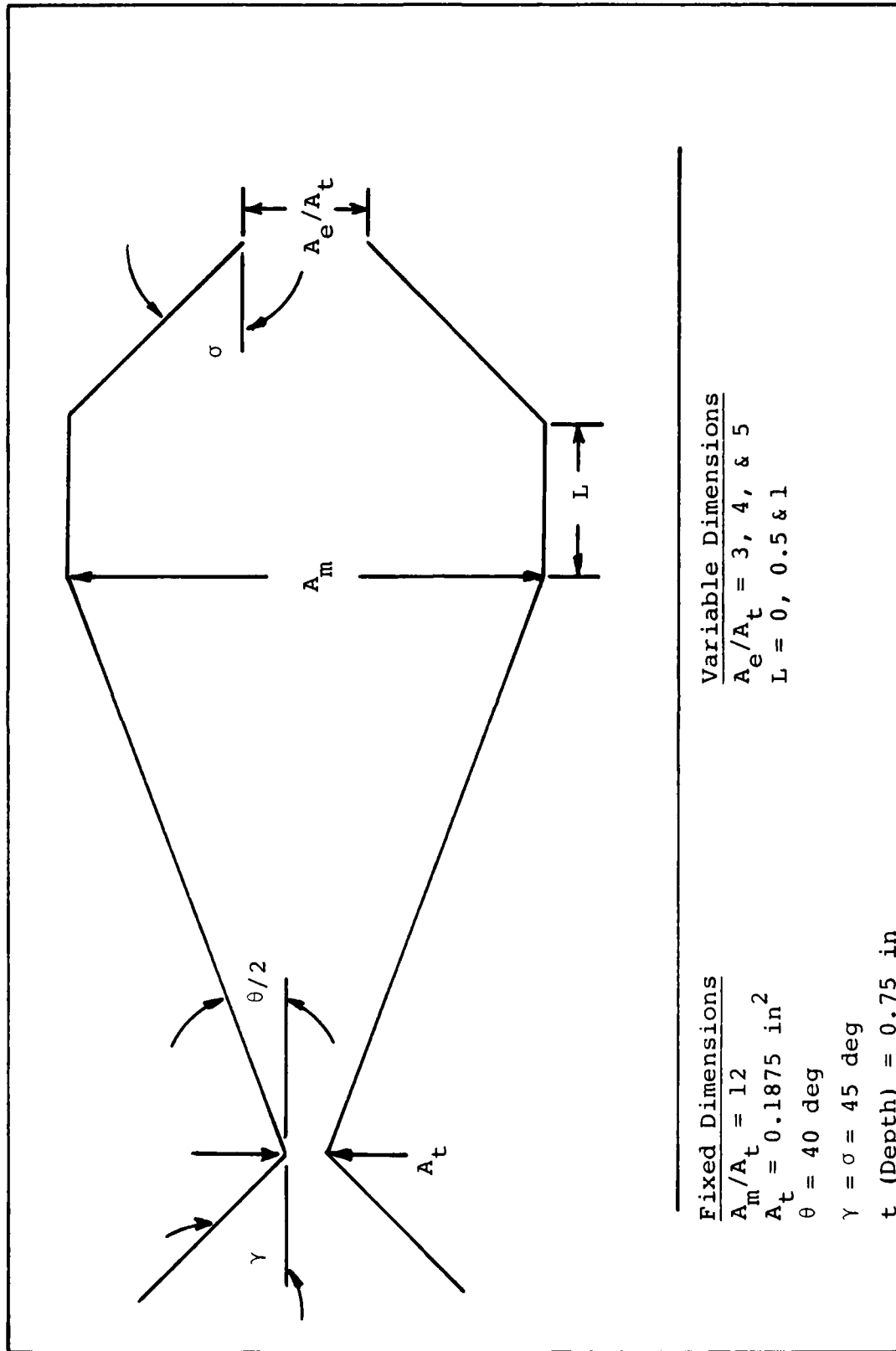


Figure 3. Nozzle Schematic

location was some distance upstream of the wall separation point. Assuming that this was also true for the two-dimensional case, it was necessary to determine the exact location of wall separation. Thompson (Ref 6) and Bollmeier (Ref 7) showed that this separation point can be predicted for unconfined two-dimensional nozzles by the equation:

$$d' = a \csc(\theta/2) \quad (1)$$

where

d' = separation distance along nozzle wall measured from the throat

θ = total divergence angle

$$a = (A_s/A_t - 1)t/2$$

A_s/A_t is the ratio of the cross-sectional area of the device at the separation point to the nozzle throat, while t is the throat height. A_s/A_t can be determined from the isentropic relation:

$$\frac{A_s}{A_t} = \frac{1}{M_s} \left[\frac{1 + [(k-1)/2]M_s^2}{(k+1)/2} \right]^{\frac{k+1}{2(k-1)}} \quad (2)$$

Thompson's expression for the Mach number at separation, M_s , is given by

$$M_s^2 = \frac{2}{k-1} \left[\left\{ \left[\frac{kn}{(n+2)} + 1 \right] [P_o/P_a] \right\}^{\frac{k-1}{k}} - 1 \right] \quad (3)$$

where

k = ratio of specific heats

n = velocity profile power law index

P_o = primary pressure

P_a = ambient pressure

Thompson assumed a compressible, turbulent, supersonic boundary layer with air as the working fluid in a two-dimensional straight wall device. With these assumptions, $k = 1.4$, and $n = 7$. Equation (3) simplifies to:

$$M_s = [6.17(P_o/P_a)^{0.286} - 5]^{0.5} \quad (4)$$

III. Experimental Apparatus

Test Assembly

The two-dimensional nozzle, Figure 4, was fabricated in three sections: 1) the mating section, 2) the optical framework, and 3) the plexiglass geometries with injector ports and pressure taps. The mating section served as the mounting interface between the test stand and the optical framework. The optical framework contained the optical glass used for flow visualization and served as the attachment point for the plexiglass geometries. The plexiglass geometries were sandwiched between the optical glass and pinned at the front and back ends to insure that they remained fixed during testing. There were five pressure taps located along each nozzle wall. In addition, SI ports were located on each of the nozzle halves. These ports were 0.1875 in diameter and were capped with 0.25 in hose connectors which were threaded into the wall of the nozzle. The SI ports in both nozzle walls were located at different lengths along the divergent contour to account for movement of the separation point due to the various pressures and geometries.

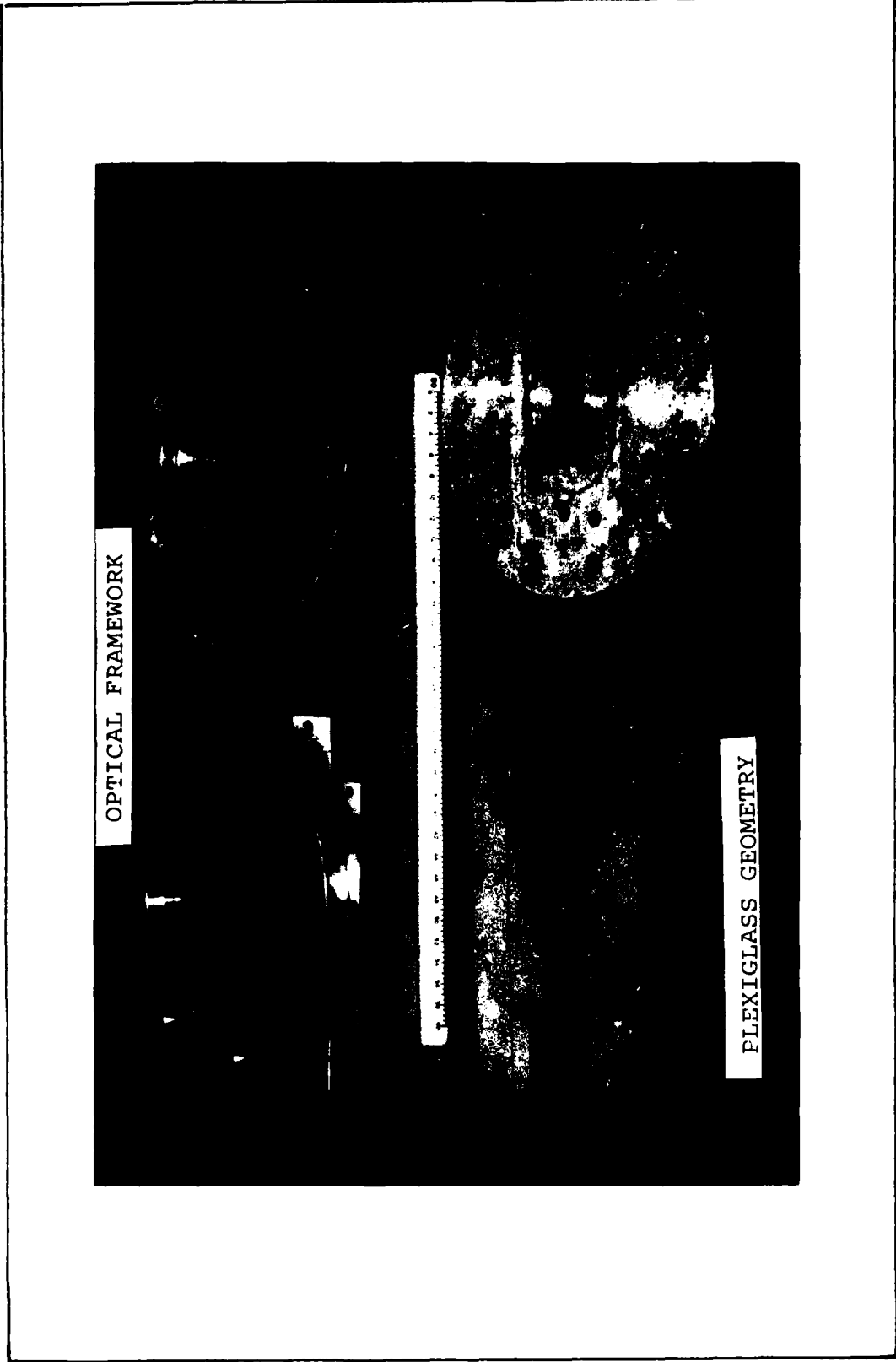


Figure 4. Nozzle Components

Plexiglass Nozzle Shapes

Nine different nozzle configurations were fabricated and tested. Figure 4 indicates a typical plexiglass nozzle geometry. The nozzles were constructed in two pieces and machined from 0.75 in plexiglass. This design was limited by the fact that each parameter variation necessitated the fabrication of new nozzle shapes.

Test Stand

Figure 5 shows a schematic of the test stand and flow measurement systems. The test assembly was mounted on a tank that serves as a settling chamber (Figures 6 and 7). This tank was mounted to a two degree-of-freedom pendulum which, in turn, was suspended from a steel gantry. A special adapter, attached to the optical framework, interfaced with a load cell anchored to the floor. This load cell, Figure 8, was instrumented with foil-backed strain gages and was used to measure both axial and side forces.

SI System and Pressure Measurement

The SI flow was supplied from a manifold that was attached to the tank by two steel bands. The manifold was attached to a venturi-tube flow meter which was used to determine SI mass flow rates. A flexible high pressure hose connected this system to a regulated air supply. Secondary flow was taken from the manifold through solenoid

valves which fed the SI ports through 0.25 in flexible tubes. Pressure transducers were mounted on a stand near the nozzle and were connected to the nozzle pressure tap by 0.0625 in flexible tubes. These transducers were bellows-type operated with an excitation voltage of 10 volts. The output of the transducers was connected to the data acquisition system.

Mass Flow Measurement

Mass flow meters were located in both the primary and secondary supply lines. The primary mass flow rate was measured with 1.125 in diameter ASME standard orifice meter. The secondary mass flow rate was obtained using a venturi-tube meter with a 0.375 in diameter venturi. A thermocouple was used to measure the fluid temperature for the mass flow measurements. The pressure taps for each meter were connected to pressure transducers which interfaced with the data acquisition system. Temperature measurements were read directly off of the thermocouple monitor.

Data Acquisition

The data acquisition system consisted of a HP3497 data storage device in conjunction with a HP85 computer. Pressure, mass flow, side force and axial thrust measurements were taken by the HP3497 and recorded on tape by the computer. The computer was capable of handling two force measurements and 17 pressure measurements from separate

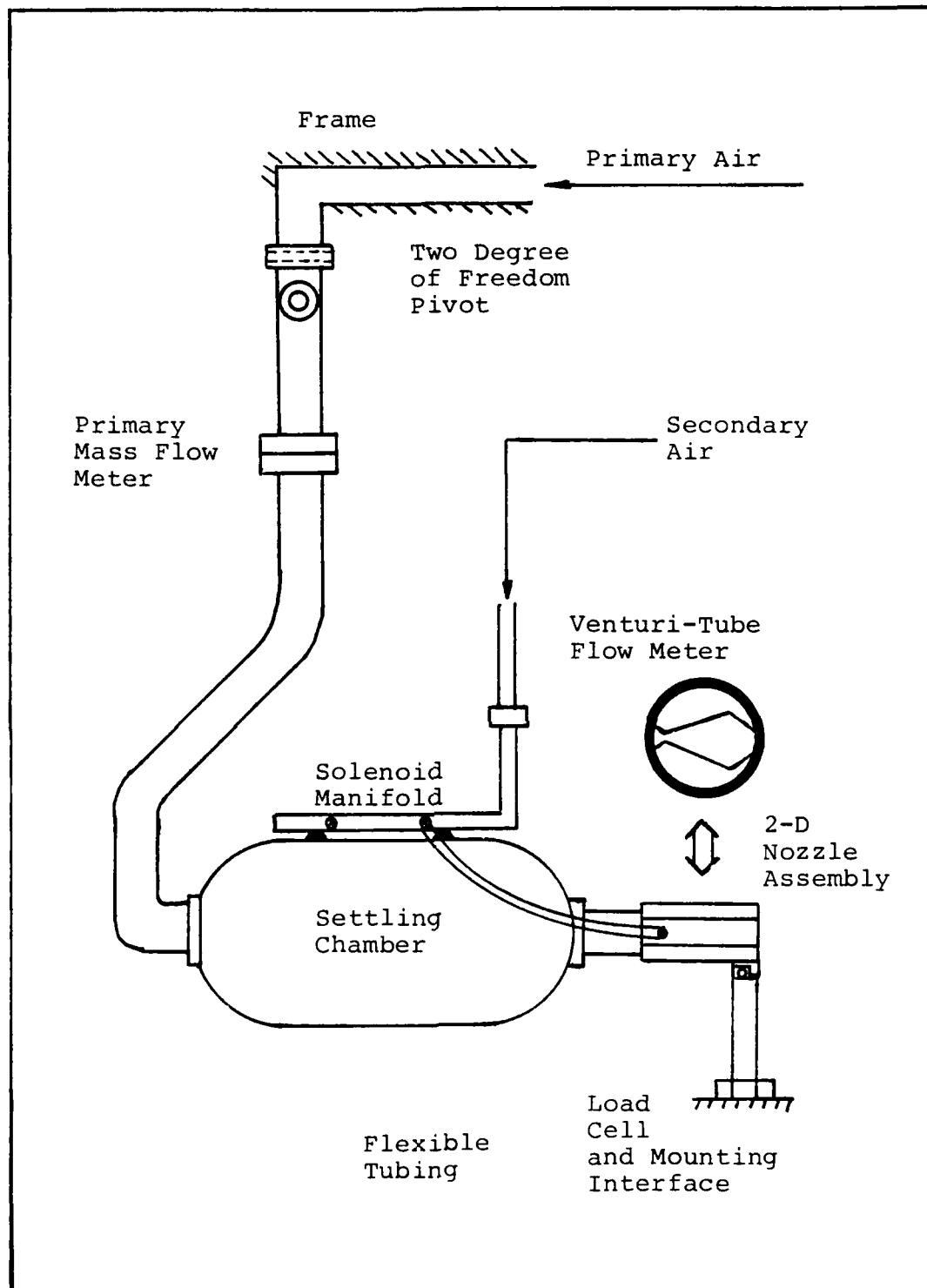


Figure 5. Test Stand Schematic



Figure 6. Nozzle Mounted on Tank/Settling Chamber



Figure 7. Nozzle Mounted on Load Cell

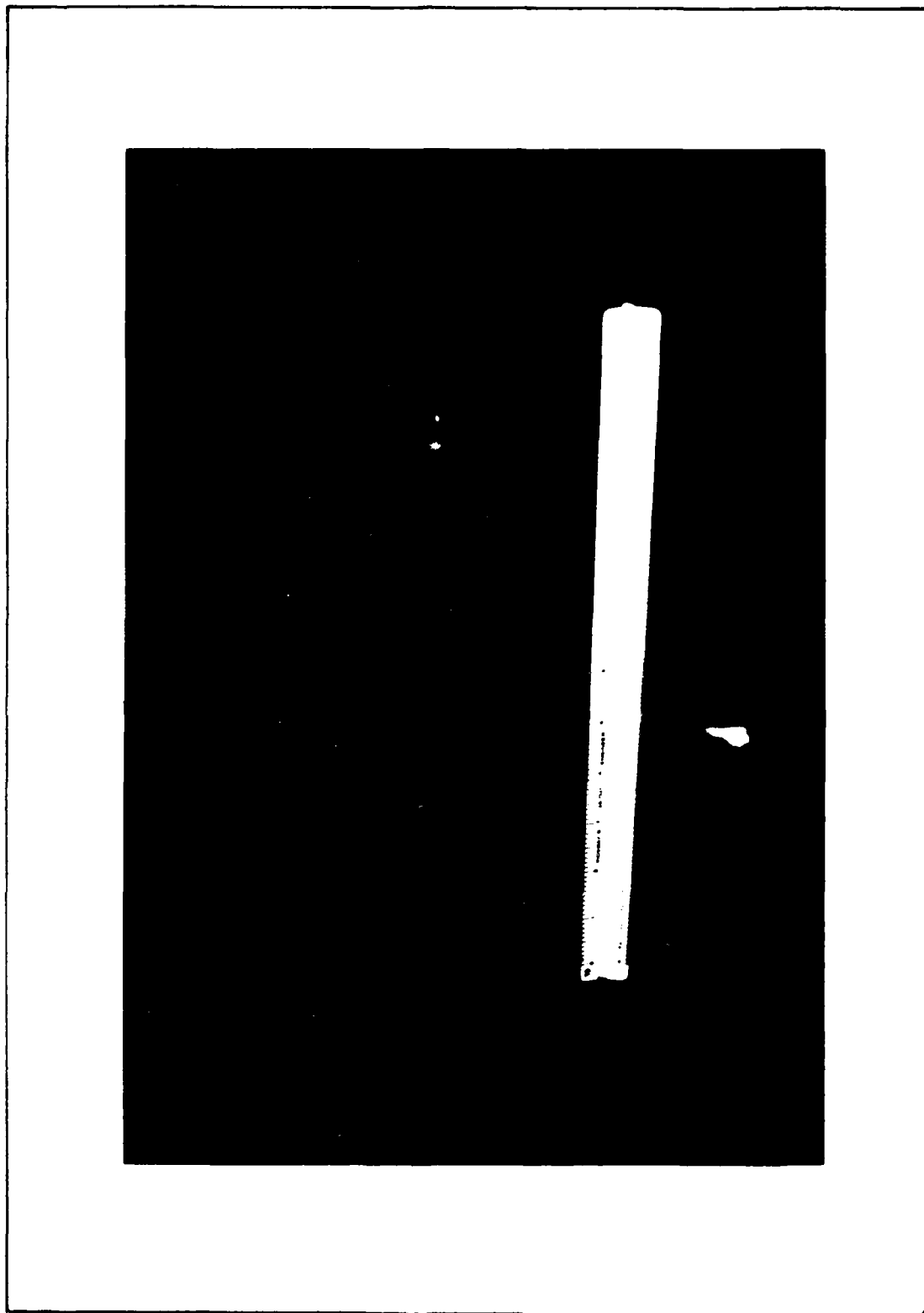


Figure 8. Load Cell

transducers. A schlieren optical system was used for flow visualization. Both high-speed movies with continuous lamp and Polaroid still pictures were obtained.

Control

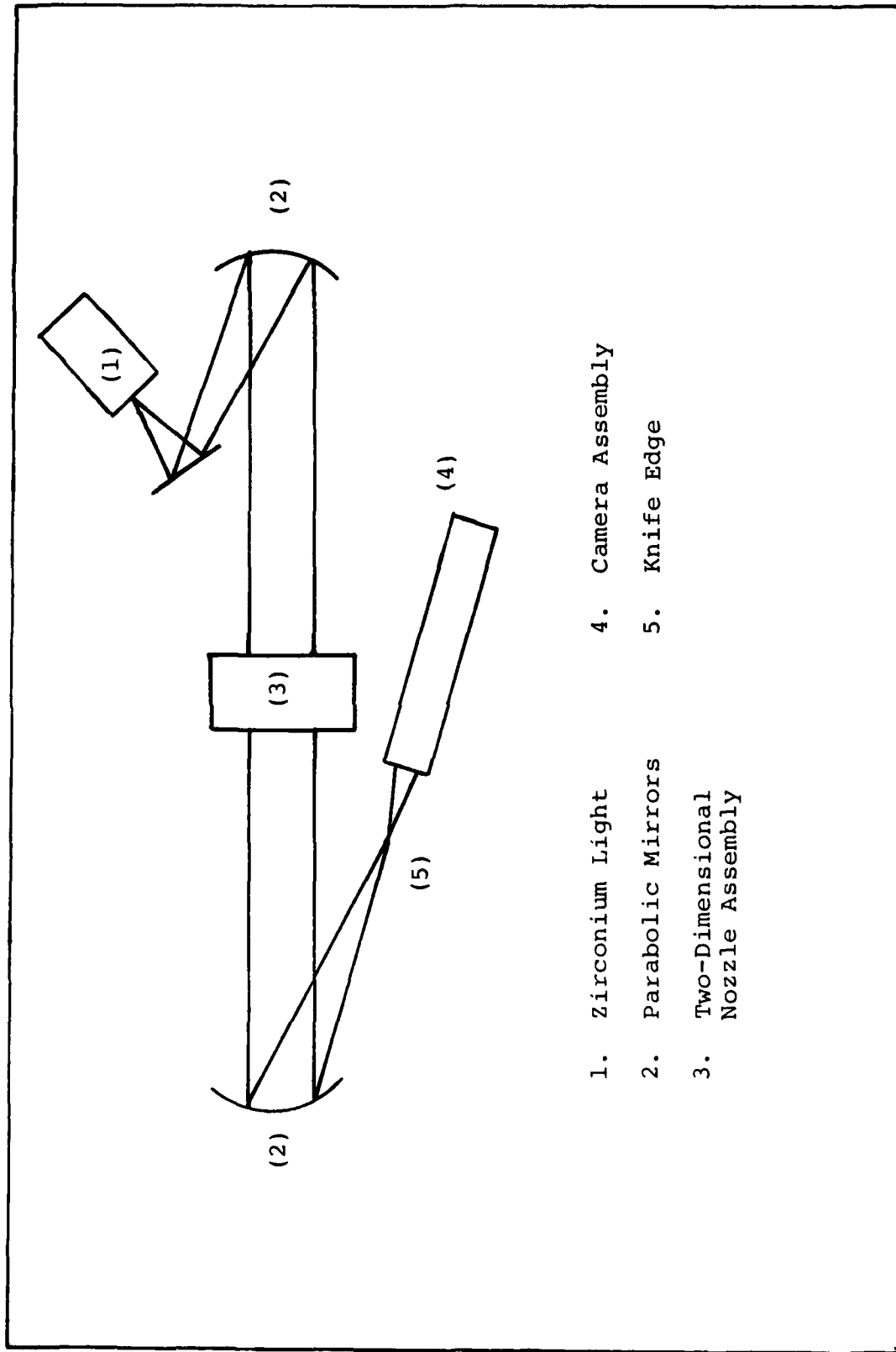
The HP85 computer was used to control the solenoid valves in the SI system. The computer was programmed to create a data file, open the desired SI valves, and record pressure, thrust, and mass flow measurements into the data file.

Control of the SI and primary supply pressures was accomplished without the computer. The primary supply was set from the control room through solenoid valves which loaded and vented dome valves in a two-stage regulator. This supply also had a remote controlled gate valve that could isolate the test stand from the supply in the event of an emergency. The SI system was controlled manually through a regulator/dome valve and was adjusted before each test run.

Flow Visualization System

The schlieren system, Figure 9, was used to obtain still photographs and high-speed motion pictures of the flow. Still photographs were taken using Polaroid type 52 (ASA 400) film with a zirconium light source.

A high-speed, 16 mm movie camera was used for motion pictures of the flow. This camera was capable of reaching



- 1. Zirconium Light
- 2. Parabolic Mirrors
- 3. Two-Dimensional Nozzle Assembly
- 4. Camera Assembly
- 5. Knife Edge

Figure 9. Schematic of Schlieren System

film speeds in the range of 6500-7000 frames per second;
however, for this application, limited light necessitated
a film speed of 24 frames per second.

IV. Experimental Procedure

The procedure for a typical test run was as follows:

1. The nozzle was configured for a specific test.
2. The SI system pressure was set through the regulator/dome valve.
3. The test area was cleared and the warning siren was activated.
4. The solenoid valve commands were stored in a data file.
5. The master control program was loaded into the computer. This enabled the computer to read the solenoid valve commands and to create a test data file based on the test time duration.
6. Ambient conditions, temperature and pressure, were recorded.
7. A calibration program was run to record the zero output values of each transducer and the load cell strain gages. This information was also used by the data viewing program to increase the accuracy of the data by comparing these values to the calibrated zero outputs of the transducers.
8. On command from the computer, the primary supply system was activated.

9. When the primary supply system reached the desired pressure, the computer was commanded to start the test.

10. At the end of a test, on command from the computer, the primary supply dome valves were vented manually by the operator to shut off the air supply.

11. The SI system was shut off and data were recorded by the computer on tape.

After a test run, thrust, pressure, and mass flow data could be viewed directly using a data viewing program. This program read the transducer levels, solenoid valve configuration and used recorded transducer characteristics to find the actual thrust, primary/secondary mass flow and pressures.

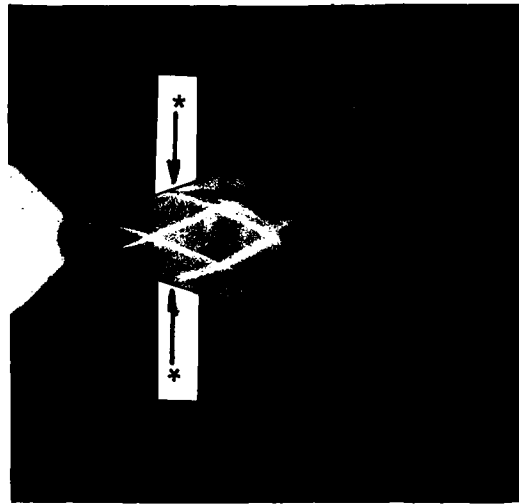
V. Results and Discussion

Separation Characteristics

Determination of Separation Points. Wall separation points were determined from the schlieren photographs as indicated in Figure 10. Separation was considered to be the point where the oblique shock intersected the nozzle wall.

Comparison with Previous Studies. The separation points of the two-dimensional nozzle are shown in Figure 11 and were compared with those of Thompson (Ref 6) and Bollmeier (Ref 7). Table I shows the pressures along the nozzle walls for several of the test configurations. Figure 12 is provided to aid in interpretation of these results. Pressure data was not available for all test configurations because of a failure of the test assembly which rendered all the pressure transducers inoperable.

The addition of the reconvergent section tends to drive the separation point toward the nozzle throat. The reconvergent section causes a pressure rise in the separation region surrounding the jet. As exit-to-throat area ratio decreases, the relative pressure within the separation region increases. Therefore, the separation distance decreases with decreasing exit-to-throat area ratio (A_e/A_t).



$A_e/A_t = 4$
 $L = 0$
 $P_o = 100 \text{ psig}$

* Separation



$A_e/A_t = 4$
 $L = 0$
 $P_o = 200 \text{ psig}$

Fig. 10. Nozzle Wall Separation

TABLE I
WALL PRESSURE DATA

Nozzle	P_o (psig)	Location													
		0	2	3	4	5	6	7	10	11	13	14	15		
$A_e/A_t=3$ L=1.0 in (Vectored to top wall)	100	28	26	23	22	32	25	25	30	35	34	27	31		
	150	40	36	32	31	45	35	35	43	48	49	38	42		
	200	52	46	42	40	58	45	44	57	61	65	50	52		
$A_e/A_t=4$ L=0 (axial)	100	11	17	16	18	16	19	17	*	17	*	*	*		
	200	27	27	30	28	31	30	34	8	35	*	*	*		
$A_e/A_t=4$ L=0.5 in (Vectored to lower wall)	100	15	20	20	28	*	34	*	*	17	19	31	19		
	150	18	27	27	40	*	46	*	*	23	26	43	27		
	200	24	34	36	51	*	59	*	*	30	35	58	35		
$A_e/A_t=4$ L=1.0 in (Vectored to lower wall)	100	13	17	20	28	18	34	15	15	17	17	*	*		
	150	17	29	22	40	25	48	24	41	24	26	*	*		
	200	22	31	38	51	33	60	31	54	31	34	*	*		

NOTE: * = not used.

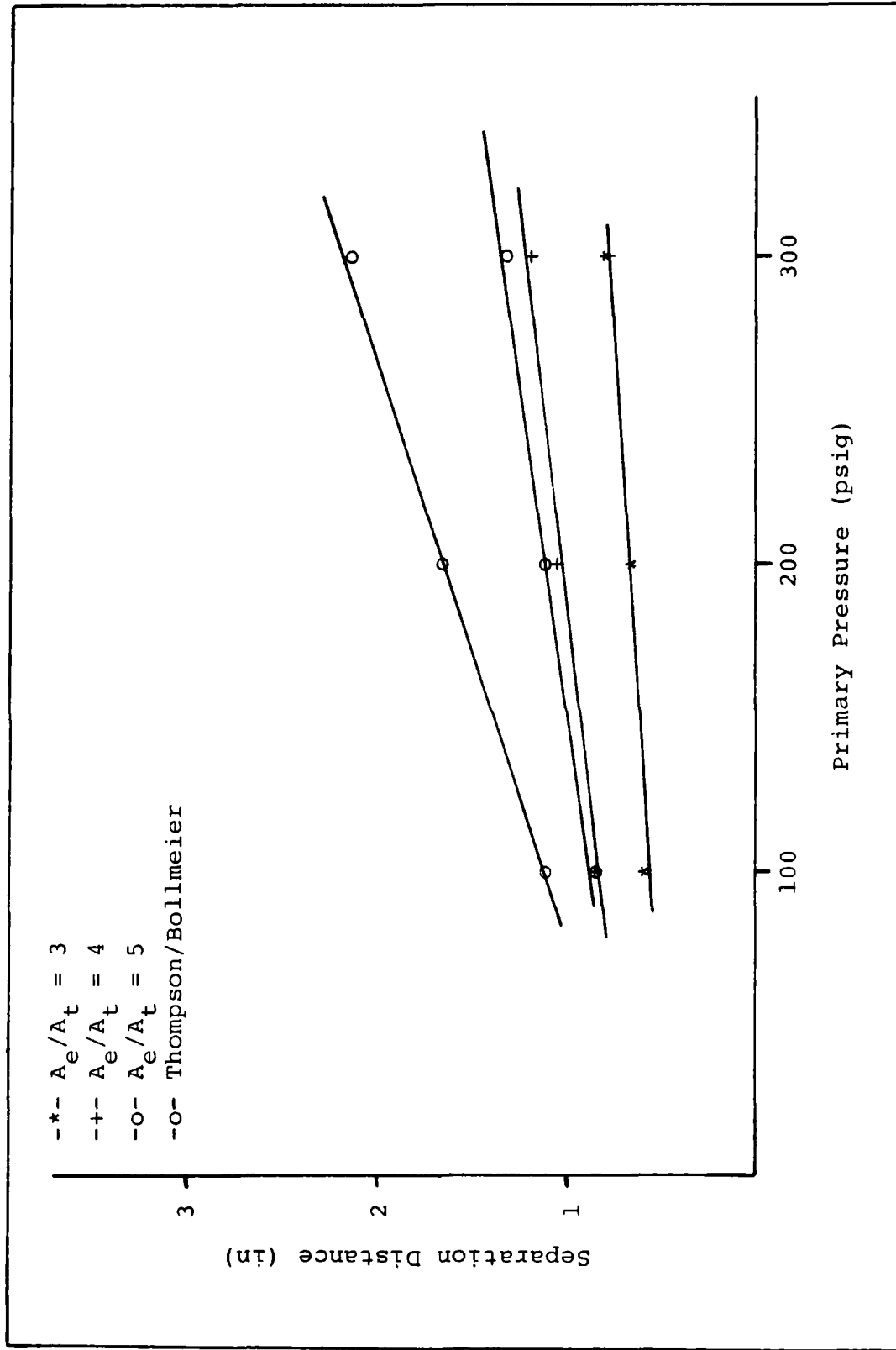


Figure 11. Separation Distance Comparison

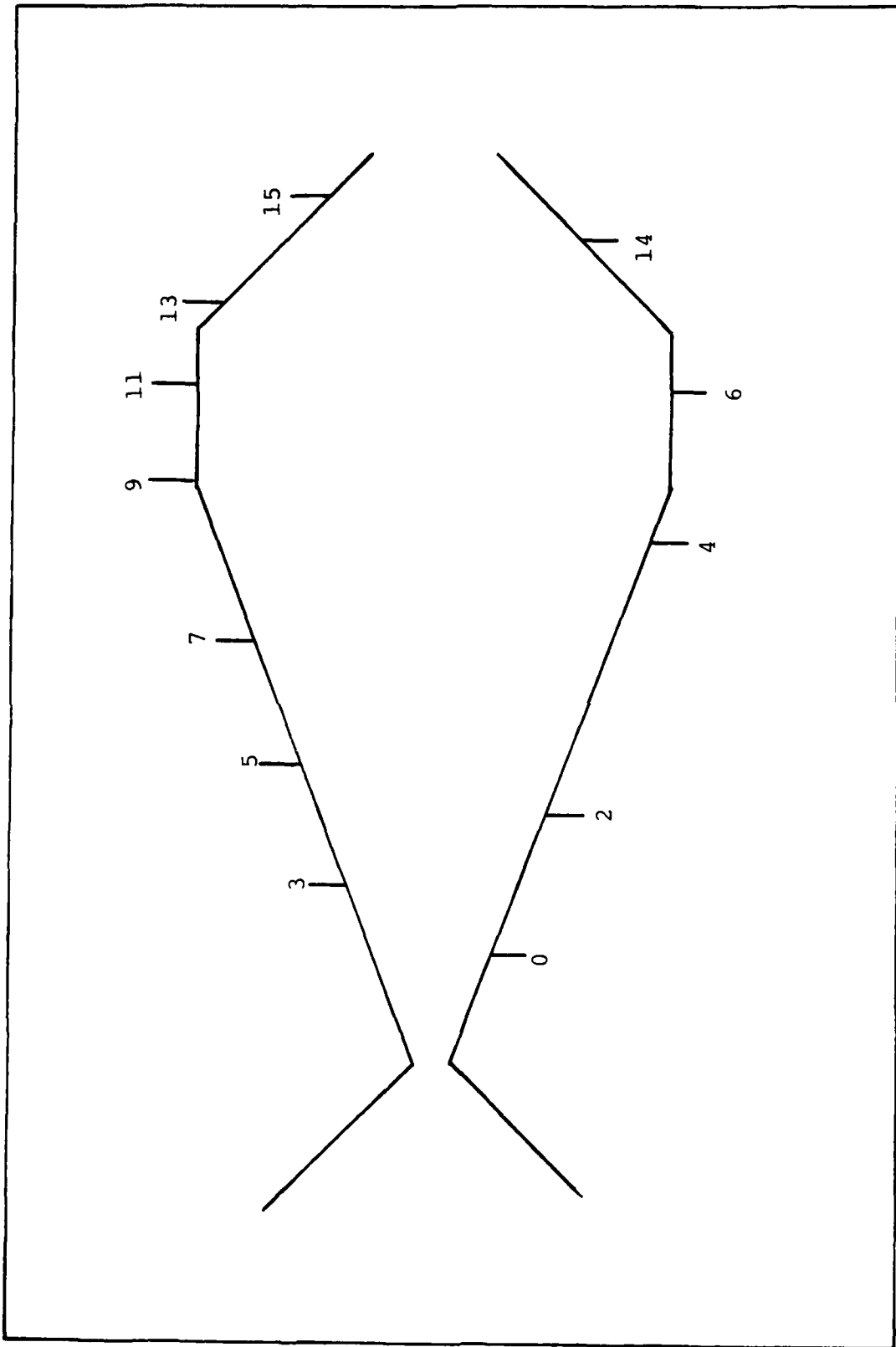


Figure 12. Schematic of Pressure Tap Locations

Nozzle Instabilities and Operating Modes

Each nozzle configuration exhibited unique modes of operation. Table II lists the various test configurations and their applicable operating characteristics. This table indicates whether the nozzle was stable, oscillatory, switchable or nonswitchable. Stability was defined as a nozzle operating in either an axial or vectored condition with no measurable force transients. Oscillatory flows were those which oscillated between nozzle walls. Switchable and nonswitchable defined whether it was possible to switch once it was vectored or to vector an axial flow.

In every case, except for the nozzle with $A_e/A_t = 4$ and $L = 0$, the flow was vectored and stable over the range of primary pressures examined. Attachment for each nozzle was random and did not favor either wall; therefore, nozzle asymmetry does not appear to be the primary cause. Each nozzle experienced an unstable oscillatory mode as the pressure was raised to the test pressures. In this mode, the jet oscillated between both nozzle walls. As the primary pressure was raised above this point, the flow stabilized but remained attached to whichever wall it was attached to as the instability was passed. At this point, nozzle operation depended upon which exit-to-throat area ratio was being tested. The nozzle with $A_e/A_t = 4$ and $L = 0$ was the only nozzle that could be operated successfully with secondary injection.

TABLE II
NOZZLE OPERATING MODES

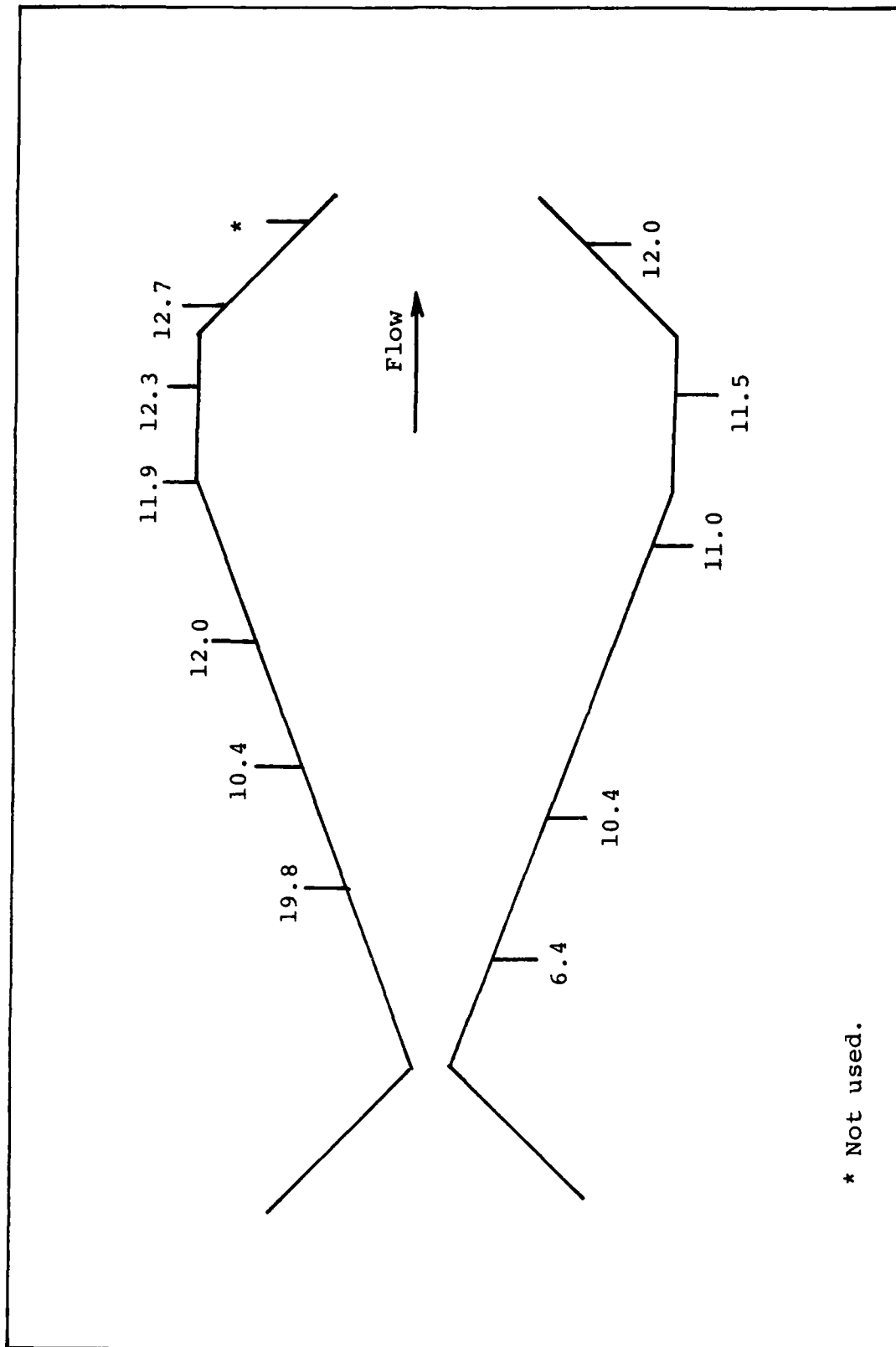
Nozzle	Modes
$A_e/A_t = 3$	L = 0 in - Unstable/Oscillatory below 50 psig - Stable/Attached above 50 psig
	L = 0.5 in - Oscillatory below 20 psig Stable above 35 psig Switchable 35 to 50 psig
	L = 1.0 in - Same as L = 0.5 in
$A_e/A_t = 4$	L = 0 in - Oscillatory at 75 psig Axial/Stable above 90 psig Switchable at 150 psig
	L = 0.5 in - Oscillatory 70 to 75 psig Can be forced axial but not consistently
	L = 1.0 in - Stable Attached over entire pressure range
$A_e/A_t = 5$	L = 0 in - Stable/Switchable 0-50 psig Oscillatory 50-70 psig Attached/Stable above 75 psig
	L = 0.5 in - Same as L = 0 in except: Stable/Attached 75-150 psig Stable/Axial/Not switchable 150-200 psig
	L = 1.0 in - Same as L = 0.5 in

Exit-to-Throat Area Ratio Effects on Flow Stability.

Figure 13 shows pressure data for a nozzle with $A_e/A_t = 5$ operating at a primary pressure of 100 psig and SI pressure of 60 psig. This nozzle was initially vectored. SI was used to drive the flow axially and then an attempt was made to vector the back to the wall on which it was attached.

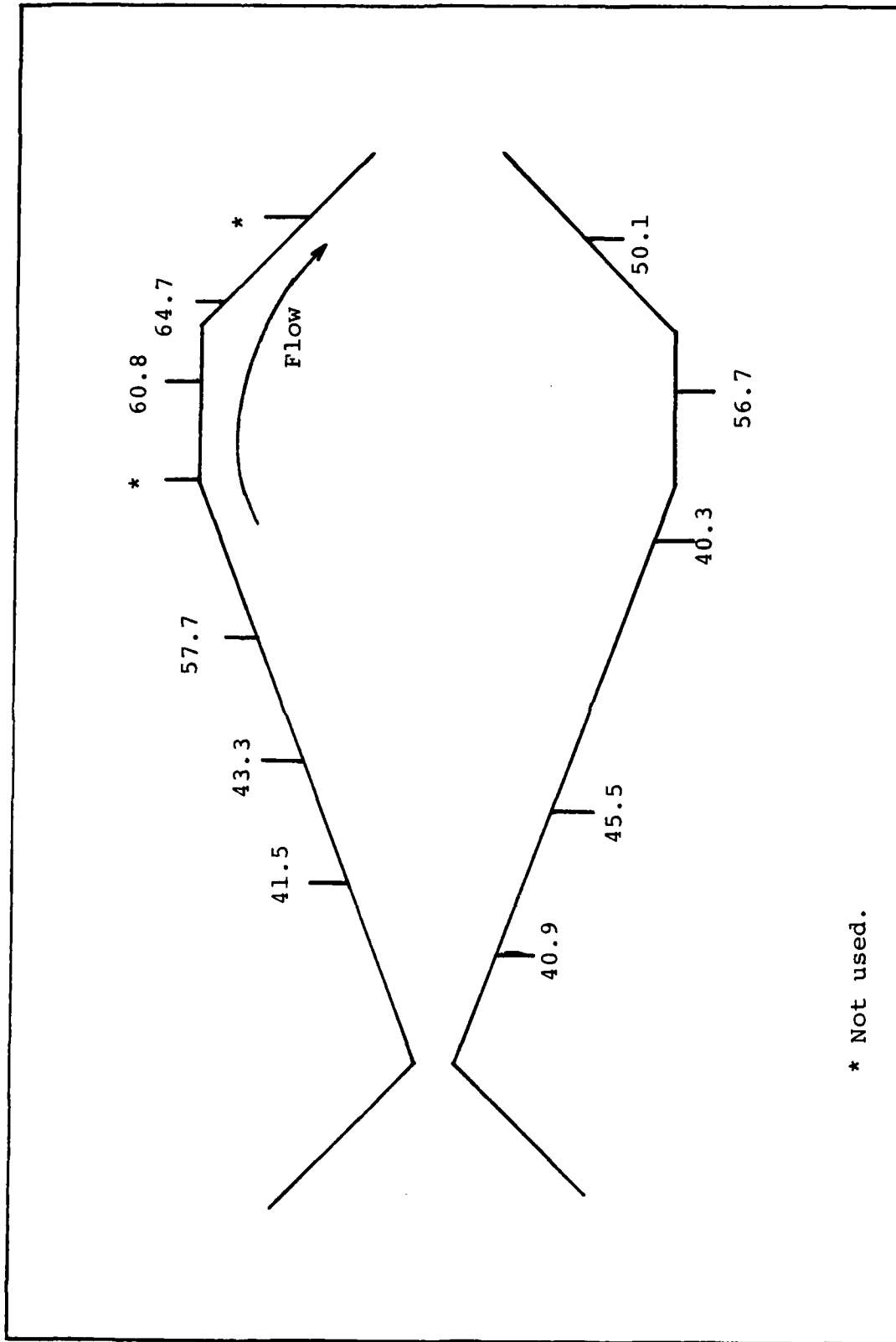
Nozzles with $A_e/A_t = 4$ and 5 could be driven axially by SI from the wall on which the flow was attached as was done in Figure 13. However, once the flow was forced axially, further attempts to vector with SI (< 100 psig) could not drive the flow to wall attachment. This can be attributed to the fact that, at these area ratios, the flow is not totally confined. Schlieren photographs of these nozzles indicated that, at $A_e/A_t = 4$ and 5, the axial jet was smaller than the exit orifice. As such, use of SI did not result in an increase in pressure in the separation region sufficient to cause vectoring. Figure 13 shows that the pressure in both separation regions remains essentially constant.

Figure 14 shows a typical pressure distribution for a nozzle with $A_e/A_t = 3$. Figure 15 shows schlieren photographs of this nozzle. Nozzles with this area ratio could not be driven axially with any amount of SI (10 to 100 psig). This can be attributed to pressure effects inside the nozzle. With this area ratio, as Figure 14 shows, the



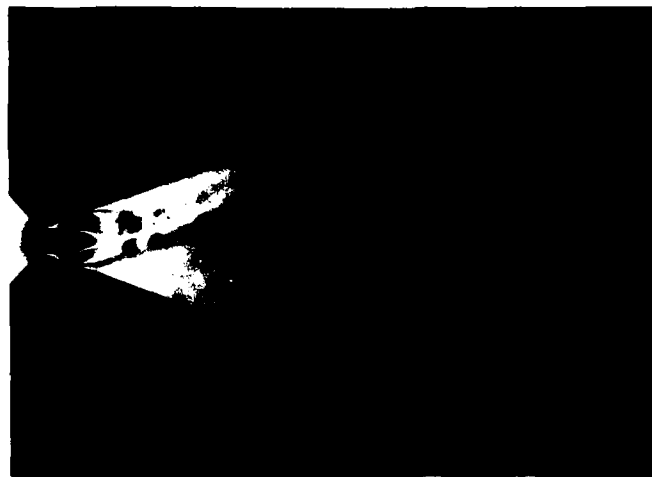
* Not used.

Figure 13. Pressure Profile for $A_e/A_t = 5$ with SI



* Not used.

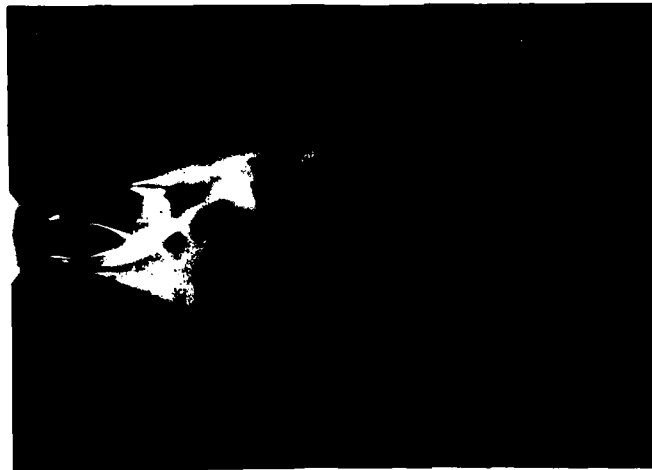
Figure 14. Pressure Profile for $A_e/A_t = 3$



$P_0 = 100$ psig



$P_0 = 150$ psig



$P_0 = 200$ psig

Figure 15. Schlieren Photographs for $A_e/A_t = 3$ Nozzle

pressure in the separation region was too high for SI to cause vectoring.

Figure 16 illustrates a mode of operation peculiar to $A_e/A_t = 5$ nozzles. Attempts to use SI with these nozzles resulted in side force being developed in a manner similar to a BLTVC nozzle.

SI Effects on Vectored Flows. Figure 17 illustrates the effect of using SI on an attached flow. Use of SI on nozzles which were initially attached could only be used to drive the flow axial. Injecting in a manner so as to push the flow against the attached wall degraded the performance of the nozzle. The SI flow acted as a wedge which disrupted the flow in the nozzle. With sufficiently high SI pressures, it was possible to cause the flow to become subsonic in the separation region.

Geometric Effects on Vector Forces and Angles

As was mentioned previously, the flow in most test configurations was attached over the entire range of primary pressures. As a result, SI could not be used for flow switching. Despite this, it was possible to examine geometric effects on side and axial forces and vector angles by examining the flows in their attached conditions.

Effects of Varying Axial Length. Table III lists axial force, side force and α for the various lengths

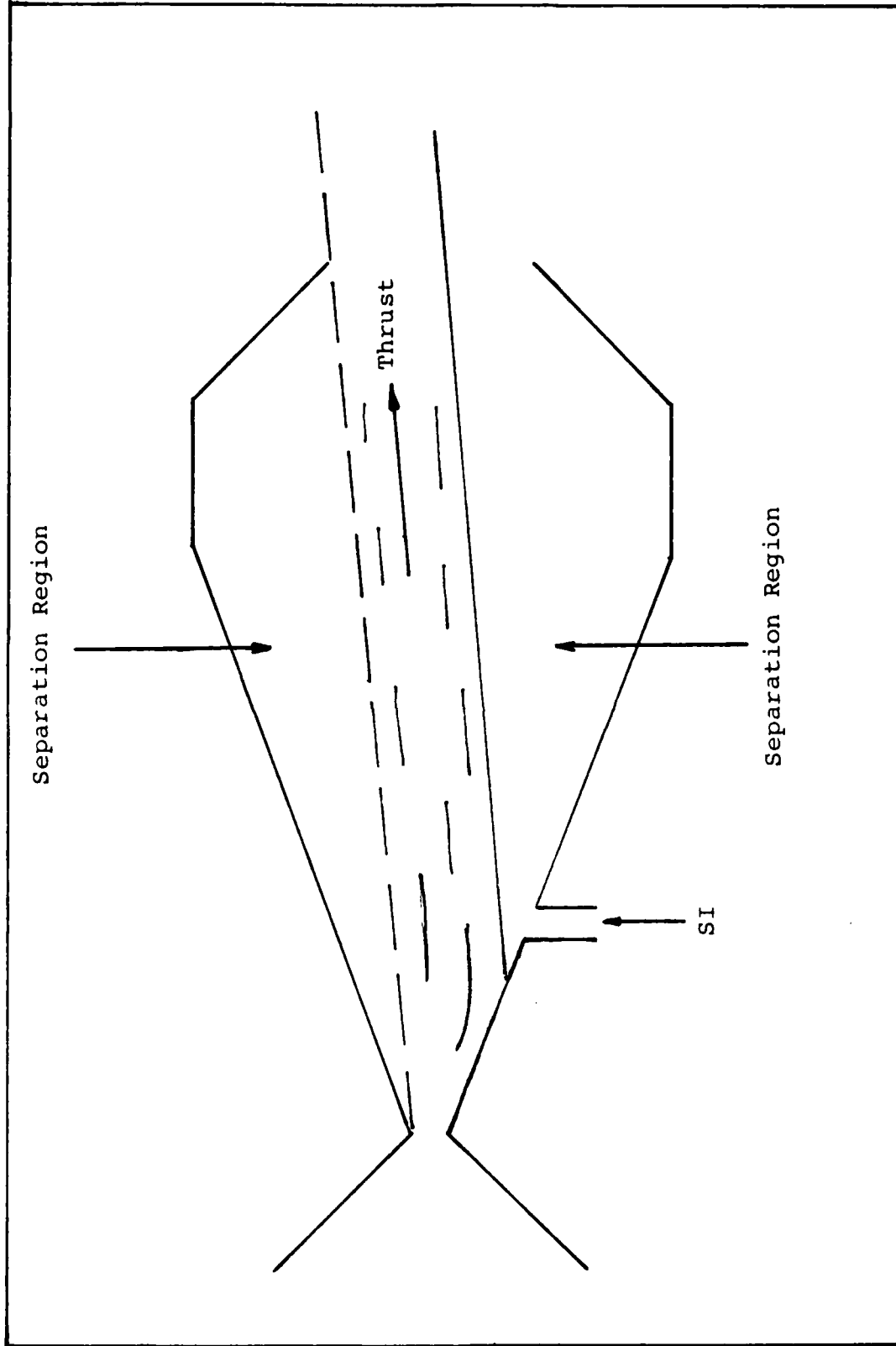


Figure 16. SI Effect on $A_e/A_t = 5$ Nozzle

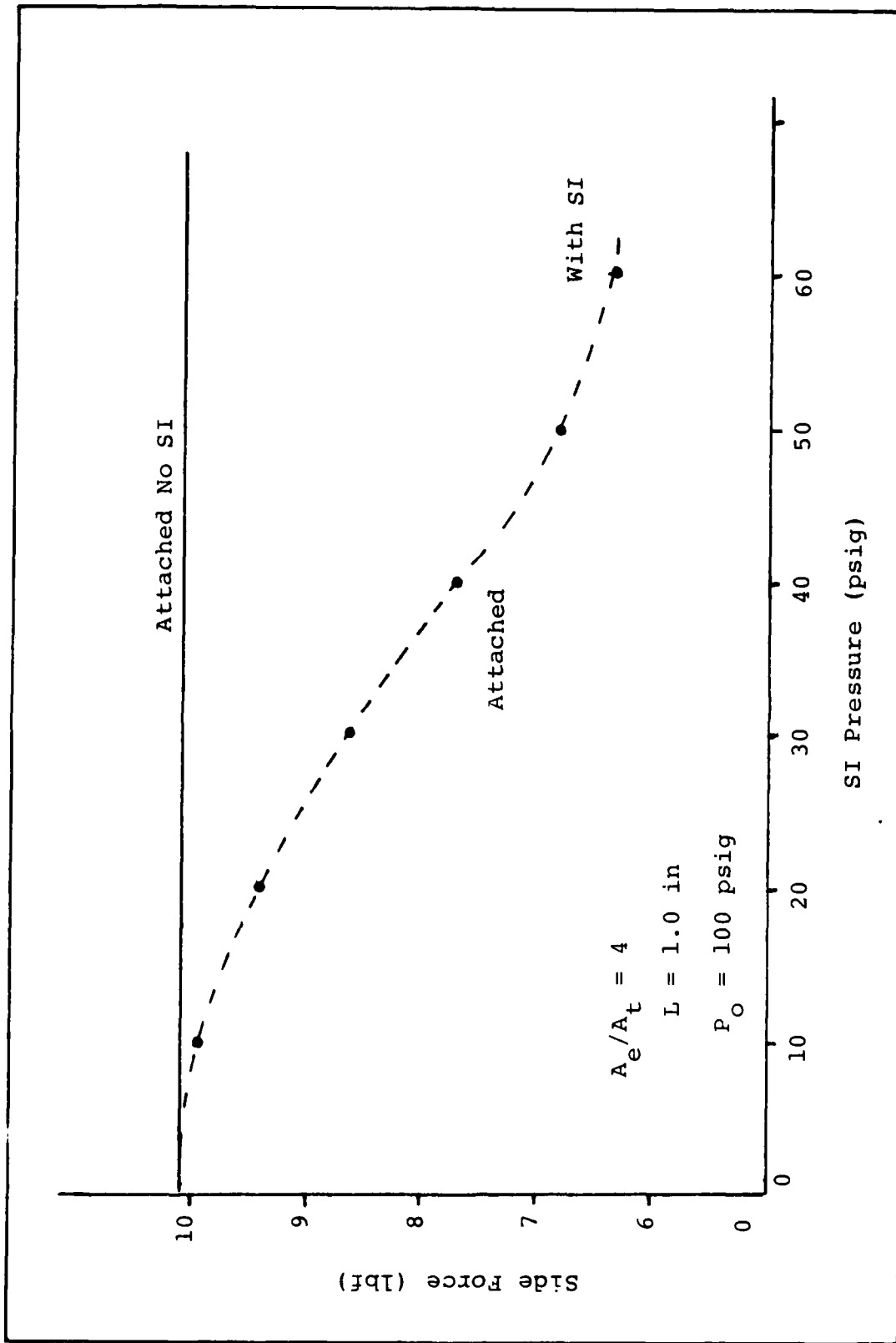


Figure 17. SI Effect on Side Force for Attached Flows

TABLE III
 AXIAL LENGTH EFFECTS ON OPERATING PARAMETER

P_o (psig)	A_e/A_t	L (in)	Axial Force (lbf)	Side Force (lbf)	α (Deg)
100	3	1.0	16.85	7.25	23.3
		0.5	17.90	7.19	21.9
		0	17.17	7.44	23.4
	4	1.0	14.01	10.51	36.9
		0.5	14.70	10.54	35.6
		0	17.00	*	*
	5	1.0	12.01	12.89	47.0
		0.5	12.42	11.61	43.1
		0	12.42	11.73	43.3
150	3	1.0	27.84	10.54	20.7
		0.5	30.01	10.52	19.3
		0	27.58	11.02	21.8
	4	1.0	25.23	16.26	32.8
		0.5	24.81	15.73	32.4
		0	29.29	*	*
	5	1.0	27.07	*	*
		0.5	23.39	17.27	36.4
		0	23.37	17.54	36.9
200	3	1.0	38.25	13.89	19.9
		0.5	42.22	13.67	17.9
		0	40.69	14.86	20.1
	4	1.0	36.76	21.19	29.9
		0.5	36.56	21.29	30.2
		0	42.86	*	*
	5	1.0	39.25	*	*
		0.5	35.23	22.54	32.6
		0	44.80	*	*

NOTE: * = Axial flow operation.

tested. Axial length variations, $L = 0, 0.5, \text{ and } 1.0$ in, were examined for each exit area. In all cases, axial force, side force, and α remained essentially constant for a given primary pressure and exit area.

Effect of Varying Primary Pressure. Figures 18, 19, and 20 illustrate the effect of varying primary pressure on axial force, side force and α . Varying primary pressure, holding A_e/A_t constant, resulted in linear changes in axial and side force and vector angle. Axial and side force increased with primary pressure while vector angle decreased. The highest axial forces were obtained with $A_e/A_t = 3$; however, at a given primary pressure there was very little difference in axial force. Highest side forces were obtained at $A_e/A_t = 5$. Side force values for $A_e/A_t = 4$ and 5 appear to converge at the higher pressures. Side forces for $A_e/A_t = 3$ were consistently lower than for the other area ratios over the entire range of pressures. Maximum vector angles were obtained with $A_e/A_t = 5$. Also, vector angles appear to converge at the higher pressures. Analogous to side force measurements, vector angles for $A_e/A_t = 3$ were consistently lower than for the other nozzles. These values were obtained by averaging the parameter for the various axial lengths. This was justified due to the minimal effect of the axial length variations tested.

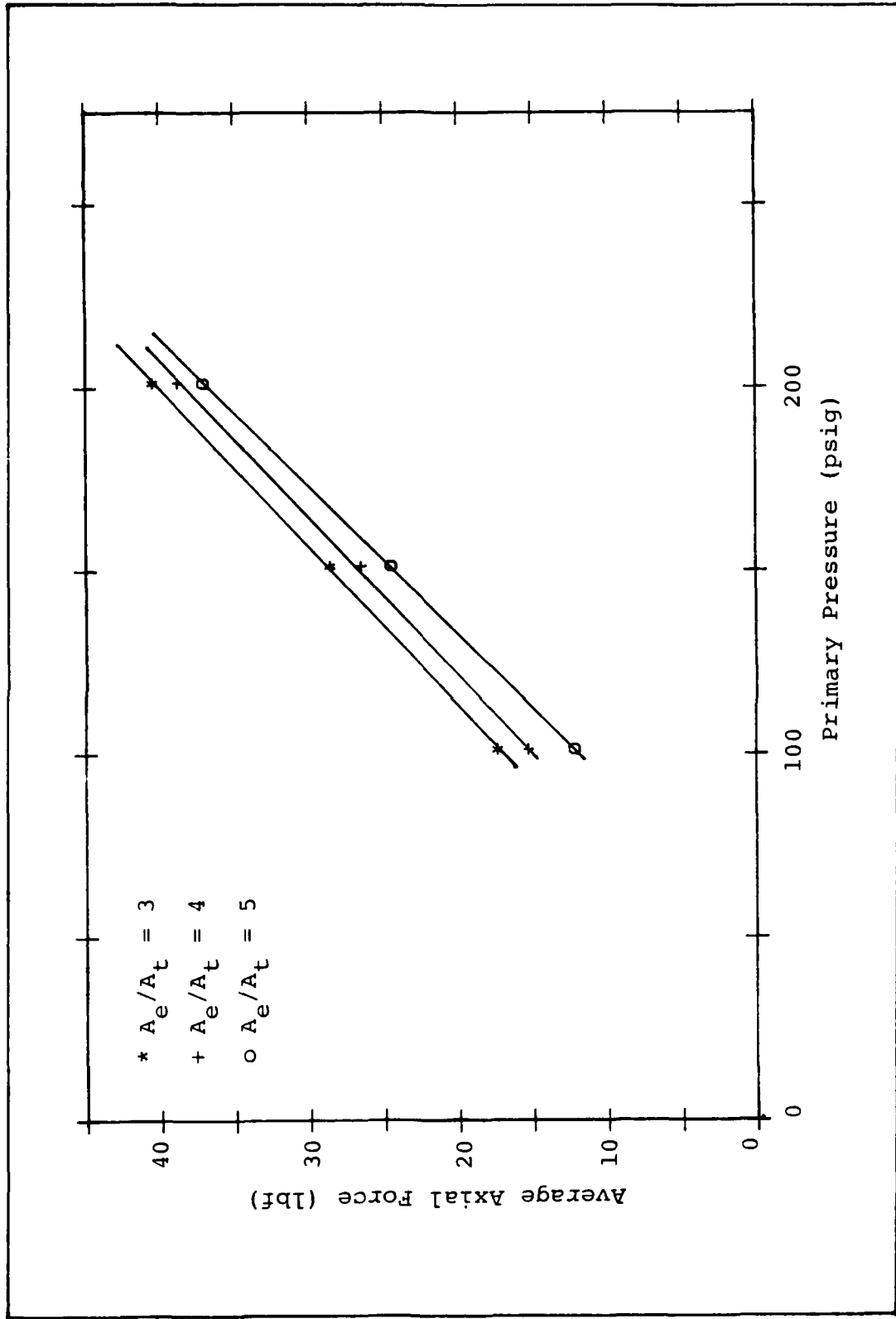


Figure 18. Primary Pressure Effects on Axial Force

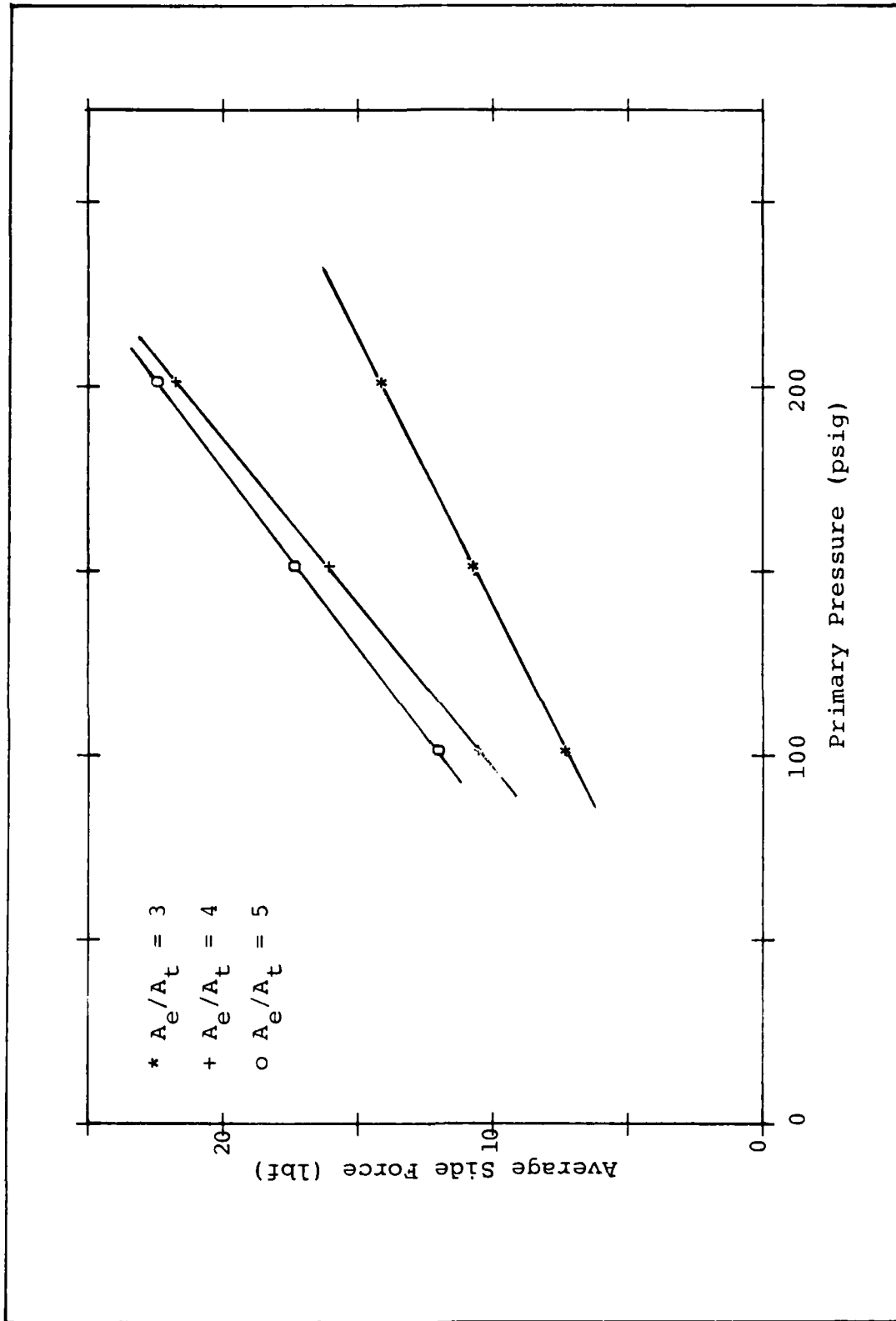


Figure 19. Primary Pressure Effects on Side Force

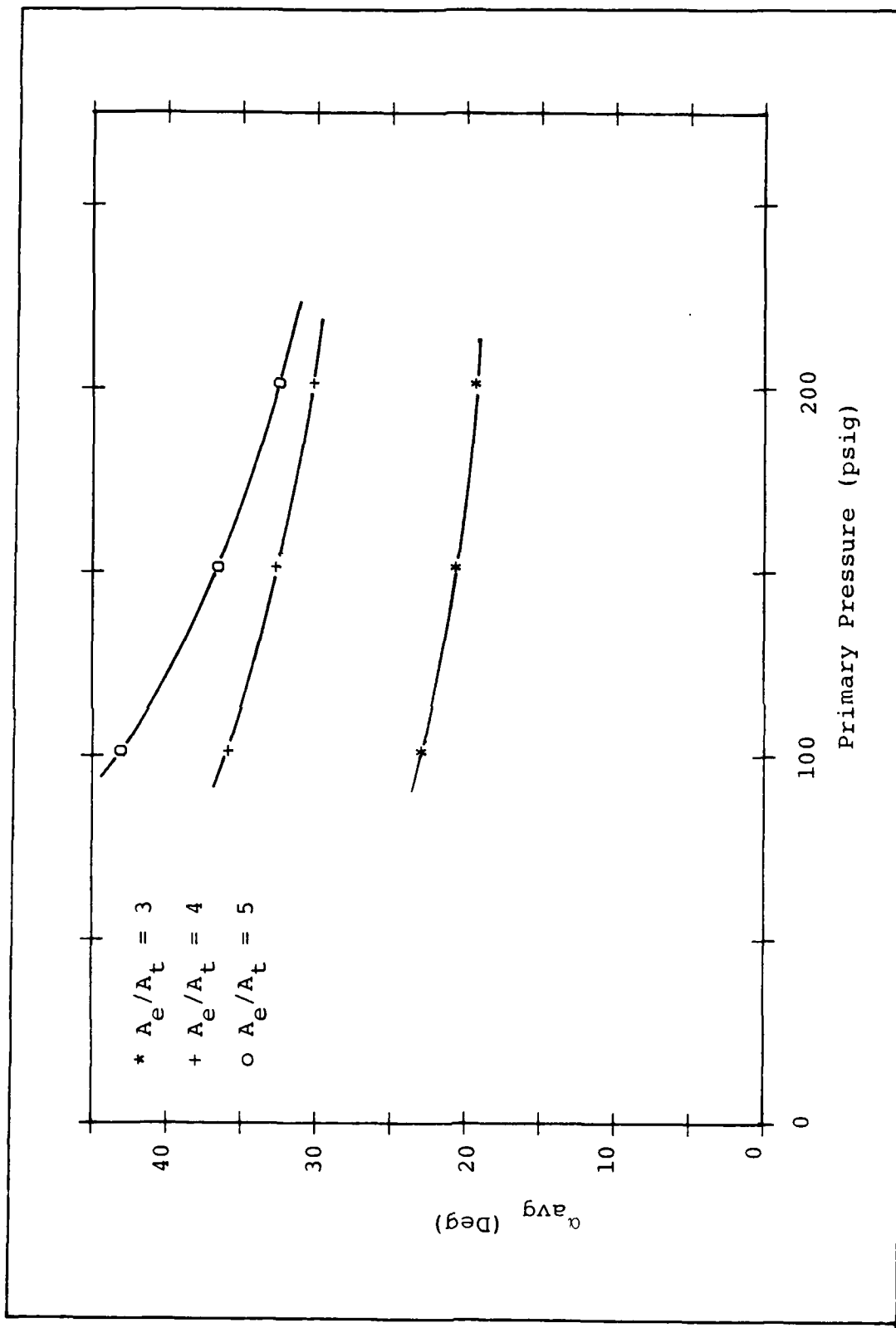


Figure 20. Primary Pressure Effects on Vector Angle

Effects of Varying Exit-to-Throat Area Ratio.

With reference to Figures 18, 19, and 20, varying A_e/A_t at constant primary pressure resulted in a linear decrease in axial force with increasing area ratio. Side force and vector angle appear to reach maximums at the higher area ratios.

Two-Dimensional CJTVC Performance

Comparison to Ideal Performance. Table IV shows a comparison between measured reaction forces, F_R , and the ideal thrust, F_I , that could be developed for each nozzle. The reaction force, F_R , was defined as the resultant force obtained by vector addition of the respective axial and side forces. Appendix B provides information on the calculation of ideal thrust along with a sample calculation. The thrust ratio, η , was defined as the ratio of F_R to F_I . This data indicates the best values of thrust ratio were obtained with $A_e/A_t = 3$. Thrust ratios were also higher at the higher primary pressures, and for a given A_e/A_t , η increased with primary pressure.

Performance with SI. The nozzle with $A_e/A_t = 4$ and $L = 0$ was the only configuration that could be switched with SI. Figures 21, 22, and 23 show effect of SI on axial force, side force, and α for this nozzle. The schlieren photographs of Figure 24 show the operation of this nozzle,

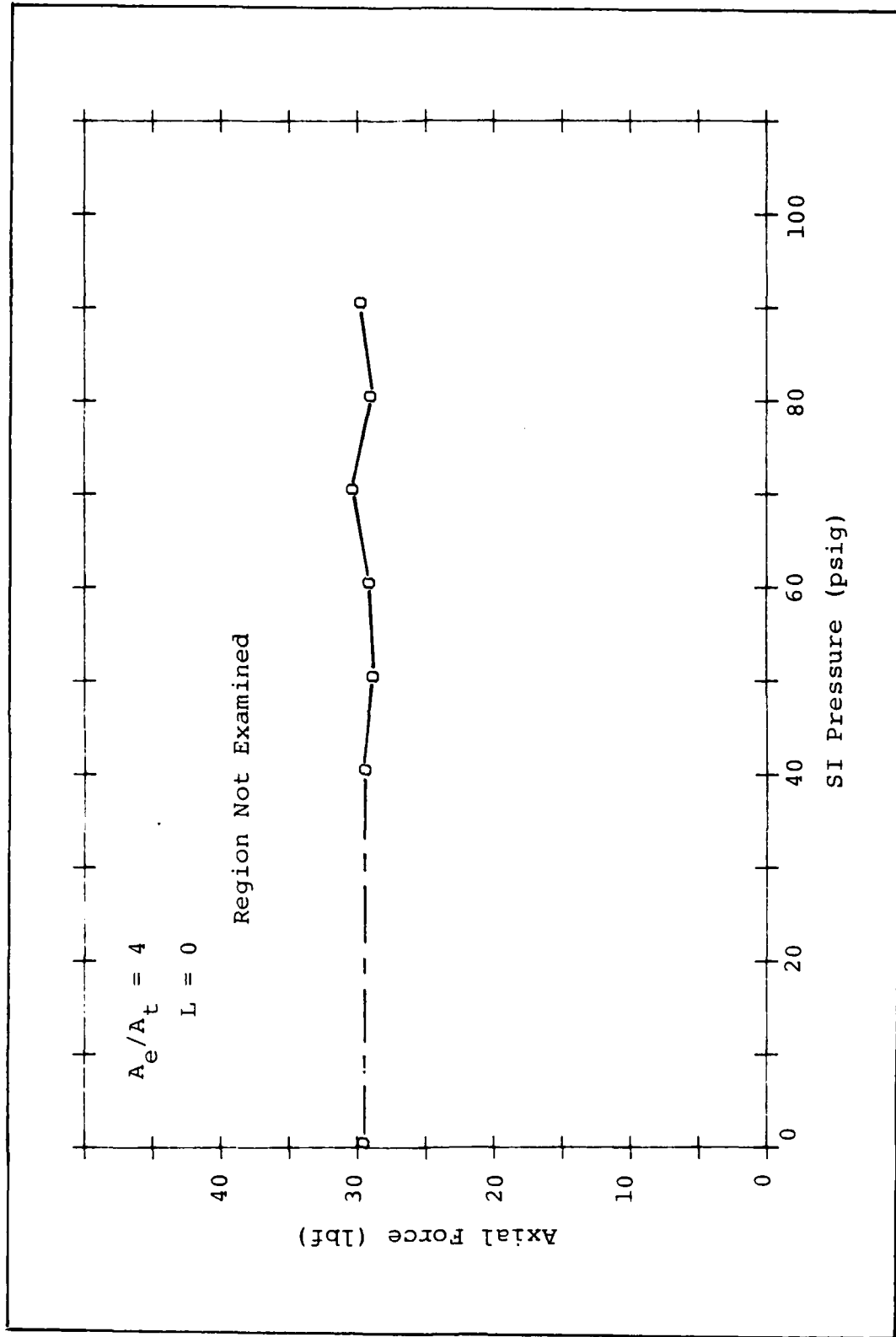


Figure 21. SI Effect on Axial Force - $A_e/A_t = 4$ and $L = 0$

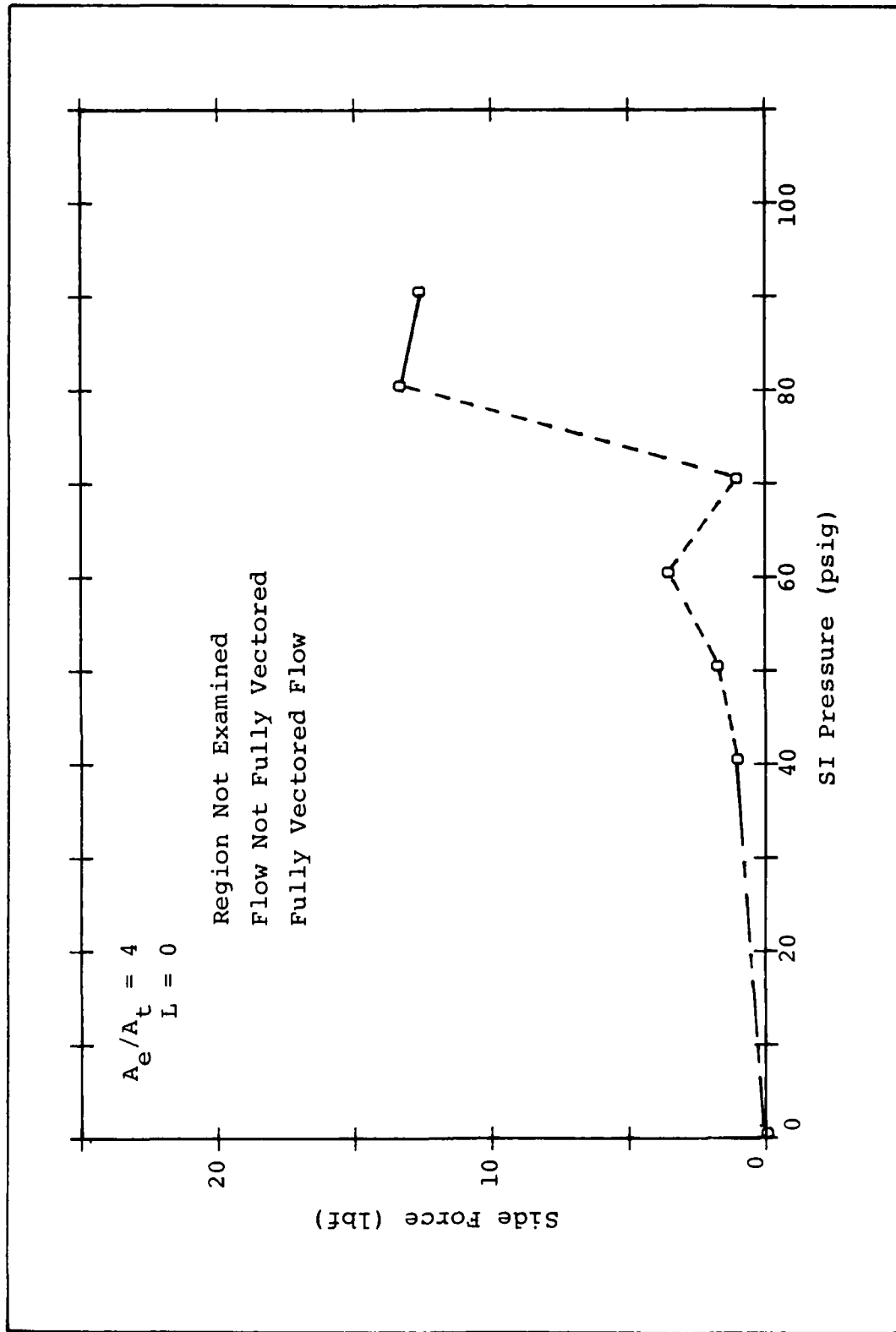


Figure 22. SI Effect on Side Force - $A_e/A_t = 4$ and $L = 0$

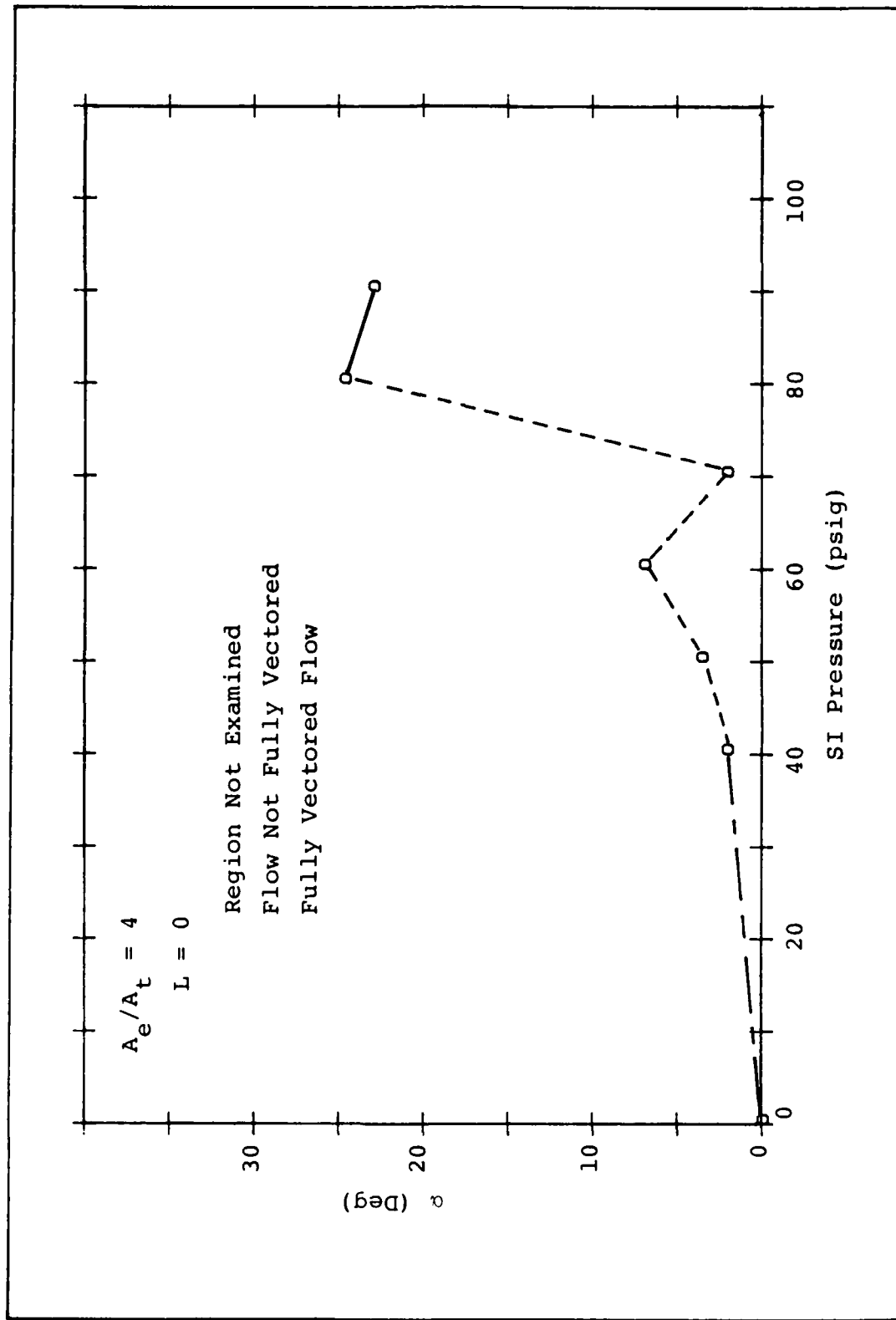


Figure 23. SI Effect on α - $A_e/A_t = 4$ and $L = 0$



$$A_e/A_t = 4$$

$$L = 0$$

Axial Flow

SI at 0 psig



$$A_e/A_t = 4$$

$$L = 0$$

Vectored Flow

SI at 80 psig

Fig. 24. Schlieren Photographs of $A_e/A_t = 4$,
 $L = 0$ Vector Operation

TABLE IV
PERFORMANCE COMPARISONS

A_e/A_t	P_a (psia)	F_R (lbf)	F_I (lbf)	η (%)
3	114.4	18.78	25.98	72.3
	164.4	30.43	39.54	79.9
	214.4	42.80	53.40	80.1
4	114.4	17.53	25.98	67.5
	164.4	30.79	39.54	77.9
	214.4	42.53	53.40	79.6
5	114.4	17.23	25.98	66.3
	164.4	28.46	39.54	71.9
	214.4	41.95	53.40	78.6

prior to and after SI activated. This nozzle was axial over the entire range of test primary pressure. Vectoring occurred only at the primary pressure of 150 psig. An SI pressure of 80 psig was necessary to vector the flow. This represents a mass flow gain (i.e. the ratio of primary mass flow rate to secondary mass flow rate) of 157.

VI. Conclusions

Based on the results of this study, the following conclusions can be drawn:

1. The theoretical equations developed by Thompson for determining separation points in unconfined nozzles do not accurately predict the separation points in confined nozzles.

2. Small axial length variations have a minimal effect on the performance of two-dimensional CJTVC nozzles.

3. Primary pressure and exit-to-throat area ratio have significant impact on two-dimensional CJTVC nozzle performance.

4. With the one nozzle configuration which could be vectored, high SI mass flow rates were needed to cause vectoring (i.e. low gain).

VIII. Recommendations

The following recommendations are made with regard to continuing this research.

1. Investigate the effects of changing wall divergence angle and axial length on flow stability.
2. Incorporate dynamic pressure transducers into the design so that the pressure behavior can be better defined.
3. Investigate the effect of enlarging the SI ports (i.e. increased SI mass flow rate) on flow switching.

Appendix A: Mass Flow Calculations

Primary Mass Flow

Primary mass flow was measured through an ASME standard orifice flow meter. For this meter, mass flow is governed by the equation:

$$\dot{m} = 0.525d^2 Y_1 K \sqrt{\rho_1 (\Delta p)} \quad (\text{A-1})$$

where

d = orifice diameter = 1.125 in

Y_1 = expansion factor = $1 - (0.41 + 0.35\beta) \frac{x}{\gamma}$

β = $d/D = 0.6$ $\gamma = 1.4$ $x = p/p$

ρ_1 = fluid density (lb_m/ft^3)

p = upstream pressure (lb_f/in^2)

K = flow coefficient

The flow coefficient, K , can be determined from the expression:

$$K = K_o (1 + A/R_d) \quad (\text{A-2})$$

where

$K_o = [(10^6 d) / (10^6 d + 15A)] K_e$

$A = d(830 - 5000\beta + 9000\beta^2 - 4200\beta^3 - \frac{530}{\sqrt{D}})$

R_d = Reynolds Number based on d

$K_e = 0.5993 + \frac{0.007}{D} + (0.364 + \frac{0.076}{\sqrt{D}}) \beta^4$

Using these relations assuming a range of Reynolds numbers from 75×10^3 to 10^7 and substituting into Equation (A-2) yields a range of K from 0.6574 to 0.6520. For this analysis an average value of flow coefficient was used.

$$K_{\text{avg}} = 0.6545 \quad (\text{A-3})$$

Substituting (A-3) into (A-1) resulted in the following expression for the primary mass flow:

$$\dot{m}_p = 0.718 \left[1 - 0.3253 \left(\frac{\Delta p}{p} \right) \right] \sqrt{\frac{p \Delta p}{T}} \quad (\text{A-4})$$

Secondary Mass Flow

A venturi-tube flow meter was used to measure secondary injectant (SI) flow rates. The venturi-tube was needed because the low SI flow rates necessitated a flow meter which was more sensitive than an orifice meter. The equation for SI mass flow was given by the following:

$$\dot{m}_{\text{si}} = D^2 I \sqrt{\Delta p \frac{p_f}{RT_f}} \quad (\text{A-5})$$

where

\dot{m}_{si} = SI mass flow (lb_m/hr)

I = Flow constant

Δp = Differential pressure across the venturi
(in H_2O)

p_f = Upstream fluid pressure (psia)

T_f = Fluid temperature

D = Inside pipe diameter = 0.625 in

The flow constant, I, was determined experimentally by calibrating the venturi-tube against a gasometer. This calibration yielded:

$$I = 21.05 \quad (A-6)$$

Substituting (A-6) into (A-5) yielded the following expression for the SI mass flow:

$$\dot{m}_{si} = 0.0038 \sqrt{\frac{\Delta p}{T_f}} \quad (A-7)$$

Appendix B: Ideal Thrust Calculation

The ideal thrust was calculated using the expression:

$$C_T = \sqrt{\frac{2k^2}{k-1} \left(\frac{2}{k+1}\right)^{\frac{k+1}{k-1}} \left[1 - \frac{P_e}{P_o} \frac{k-1}{k}\right]} + \frac{A_e}{A_t} \left(\frac{P_e}{P_o} - \frac{P_a}{P_o}\right) \quad (B-1)$$

where

C_T = thrust coefficient ($\tau/A_t P_o$)

k = Ratio of specific heats

A_e = Exit area (in²)

A_t = Throat area (in²)

P_e = Exit pressure (psia)

P_a = Ambient pressure (psia)

P_o = Supply pressure (psia)

For this ideal calculation it was assumed $k = 1.4$ and $P_e = P_a$. With these substitutions, Equation (B-1) reduces to:

$$C_T = \sqrt{3.282 \left[1 - \left(\frac{P_e}{P_o}\right)^{.286}\right]} \quad (B-2)$$

Bibliography

1. Fitzgerald, R. E. and R. F. Kampe. "Boundary Layer TVC for Missile Applications," AIAA/SAE/ASME 19th Joint Propulsion Conference, AIAA-83-1153, AIAA, New York, 1983.
2. Fitzgerald, R. E. and R. F. Kampe. Confined Jet Thrust Vector Control (CJTVC) Nozzle Development and Cold Flow Testing Program, NWCTP6126, Naval Weapons Center, China Lake CA, 1980.
3. Fitzgerald, R. E., R. F. Kampe, and R. A. Jacobson. Confined Jet Thrust Vector Control (CJTVC) Development and Testing Program, NWCTP6197, Naval Weapons Center, China Lake CA, 1982.
4. Porzio, A. J. Characteristics of Confined Jet Thrust Vector Control Nozzle. MS thesis. Air Force Institute of Technology (AU), Wright-Patterson AFB OH, December 1984.
5. Brown, B. G. Experimental Study of Three-Dimensional Confined Jet Thrust Vector Control (CJTVC) Nozzles. MS thesis. Air Force Institute of Technology (AU), Wright-Patterson AFB OH, December 1985.
6. Thompson, R. V. Theoretical Determination of the Point of Separation in a Compressible, Turbulent, Supersonic Boundary Layer Subjected to an Adverse Pressure Gradient. Paper 67-WA-FE-38. New York: American Society of Mechanical Engineers.
7. Bollmeier, W. S. and Franke, M. E. Effect of Wall Configuration on the Performance of a Supersonic Bistable Device. Paper X4. Upsala, Sweden: 5th Cranfield Fluids Conference, 13-16 June 1972.

VITA

James W. Cates was born [REDACTED] [REDACTED]
[REDACTED] He graduated from [REDACTED],
Heflin, Alabama in 1977. He entered the Georgia Institute
of Technology in September 1977, graduating with a degree
of Bachelor of Mechanical Engineering in 1981. As a gradua-
ate of the Air Force ROTC program, he was commissioned into
the Air Force and entered active duty in September 1981 and
served with the Deputy for Safety, HQ Armament Division,
Eglin AFB, Florida until entering the Air Force Institute
of Technology in May 1984.

Permanent address: [REDACTED]
[REDACTED] [REDACTED]

UNCLASSIFIED

SECURITY CLASSIFICATION OF THIS PAGE

AD A164214

REPORT DOCUMENTATION PAGE

1a. REPORT SECURITY CLASSIFICATION UNCLASSIFIED		1b. RESTRICTIVE MARKINGS	
2a. SECURITY CLASSIFICATION AUTHORITY		3. DISTRIBUTION/AVAILABILITY OF REPORT Approved for public release; distribution unlimited.	
2b. DECLASSIFICATION/DOWNGRADING SCHEDULE		5. MONITORING ORGANIZATION REPORT NUMBER(S)	
4. PERFORMING ORGANIZATION REPORT NUMBER(S) AFIT/GAE/AA/85D-2		7a. NAME OF MONITORING ORGANIZATION	
6a. NAME OF PERFORMING ORGANIZATION School of Engineering	6b. OFFICE SYMBOL (If applicable) AFIT/ENG	7b. ADDRESS (City, State and ZIP Code)	
6c. ADDRESS (City, State and ZIP Code) Air Force Institute of Technology Wright-Patterson AFB, Ohio 45433		9. PROCUREMENT INSTRUMENT IDENTIFICATION NUMBER	
8a. NAME OF FUNDING/SPONSORING ORGANIZATION	8b. OFFICE SYMBOL (If applicable)	10. SOURCE OF FUNDING NOS.	
8c. ADDRESS (City, State and ZIP Code)		PROGRAM ELEMENT NO.	TASK NO.
11. TITLE (Include Security Classification) See Box 19		PROJECT NO.	WORK UNIT NO.
12. PERSONAL AUTHOR(S) James W. Cates, B.M.E., Capt, USAF			
13a. TYPE OF REPORT MS Thesis	13b. TIME COVERED FROM _____ TO _____	14. DATE OF REPORT (Yr., Mo., Day) 1985 December	15. PAGE COUNT 66
16. SUPPLEMENTARY NOTATION			
17. COSATI CODES		18. SUBJECT TERMS (Continue on reverse if necessary and identify by block number)	
FIELD	GROUP	Two-Dimensional, Variable Geometry, Flow Visualization, Secondary Injection, Vector Angle, Axial Thrust, Side Force	
01	03		
19. ABSTRACT (Continue on reverse if necessary and identify by block number)			
Title: TWO-DIMENSIONAL CONFINED JET THRUST VECTOR CONTROL WITH FLOW VISUALIZATION AND VARIABLE FLOW GEOMETRY			
Thesis Advisor: Milton E. Franke, Professor Department of Aeronautics and Astronautics			
20. DISTRIBUTION/AVAILABILITY OF ABSTRACT UNCLASSIFIED/UNLIMITED <input checked="" type="checkbox"/> SAME AS RPT. <input type="checkbox"/> DTIC USERS <input type="checkbox"/>		21. ABSTRACT SECURITY CLASSIFICATION UNCLASSIFIED	
22a. NAME OF RESPONSIBLE INDIVIDUAL Milton E. Franke, Professor		22b. TELEPHONE NUMBER (Include Area Code) 513-255-2562	22c. OFFICE SYMBOL AFIT/ENY

Approved for public release: IAW AFR 130-17.
 Lynn E. Wolaver 16 JAN 86
 Dean for Research and Professional Development
 Air Force Institute of Technology (AFIT)
 Wright-Patterson AFB OH 45433

An experimental investigation of a two-dimensional confined jet thrust vector control nozzle was performed. The performance parameters considered were axial force, side force, and vector angle. Flow visualization was used to provide a visual record of flow behavior. Variables included primary pressure, exit-to-throat area ratio, and exit-to-throat axial length.

With each test configuration, it was possible to define specific operating modes where the flow was oscillatory, vectored/switchable, and vectored/unswitchable. Only one test configuration yielded a stable axial flow on which secondary injection could be used to study vectoring. Switchable flows existed only at low pressures below the range of test pressures making it impossible to study switching characteristics. Because the flows were attached over the entire range of test pressures, geometric effects were based on the study of these attached flows.

Results indicate that the theoretical equations for predicting wall separation points in unconfined nozzles do not accurately predict the separation points in confined jet nozzles. Small variations in axial length as examined in this study had a minimal impact on nozzle performance. Primary pressure and exit-to-throat area ratio have the most significant impact on two-dimensional nozzle performance.